Modelling tidal residual flows in the Ems Estuary

Mathijs van den Adel

May 2022

MSc thesis
Hydrology and Quantitative Water Management Group
Wageningen University

Abstract

A recent field study by Van Maren et al. [2021] aims to identify the mechanisms behind up-estuary sediment transport from the Ems estuary (The Netherlands), up the Fairway into the Lower Ems River. Tidal asymmetry at the entrance of the Fairway, downstream of the Lower Ems river, was found to be ebb-dominant. Therefore another explanation had to be found to explain the up-estuary sediment transport from the estuary towards the harbour of Emden, through the Fairway up to the lower Ems river. Van Maren et al. [2021] hypothesised about the presence of a residual water circulation cell over the Geiseleit Dam. This cell transports water from the Dollard over the Geiseleit Dam into the Fairway, and then, from the confluence zone of the Dollard and Fairway back into the Dollard. This hypothesis is based on indirect evidence, as measurements were still limited in space and time. This thesis uses numerical modelling to further assesses the hypothesis. The purpose of this assessment is to: (1) find out whether this circulation cell exists, (2) identify the main tidal barotropic mechanisms that drive this cell, and (3) find out the role of the Geiseleit dam with regard to these sub-tidal mechanisms. These three objectives were achieved by setting up a Delft Flexible Mesh model to simulate depth-averaged Eulerian velocities and water levels. The model results were used to analyse the tidal propagation by means of the M_2 tidal constituent phase and amplitude and instantaneous water heights. An analysis on the residual Eulerian velocity vectors, Stokes drift of the tidal wave, and residual Lagrangian vectors revealed the presence of a circulation cell, as was hypothesised. A key tide-induced process turned out to be a residual Stokes drift, transporting water from the Dollard into the Fairway over the Western sandbank of the Geiseleit Dam (Geisesteert) near Emden. Mass transport due to Stokes drift closes the circulation cell. An Eulerian counter current was found to partly counter the mass transport resulting from Stokes drift. However, the compensation residual current was marginal compared to the cross-dam directed Stokes drift of 7 cm/s, resulting in a net Lagrangian transport across the dam. Finally, the modelling of different dam height scenarios revealed that the presence of the dam enhances the set-up in the Dollard more than in the Fairway, leading to a greater residual transport over the Geisesteert. This as a greater setup was observed along with an enhanced the cross-dam Stokes drift.

Contents

1 | Introduction

1.1 Challenges in the Ems estuary

Anthropogenic activities in the Ems estuary, such as the dredging developments in the 1990's, have led to hyper-turbidity. The development of a hyper-turbid regime increased the need for policymakers to come up with solutions that balance economic interest, related to high dredging costs, and ecologic interests. [van der Werf, 2019, Colijn et al., 1987].

The transition to a hyper-turbid estuarine system greatly deteriorated the ecosystem of the Ems Estuary and stresses the ecology of the estuary to present day [Talke et al., 2007]. The hyper-turbid sediment regime limits primary production of biomass, constraining the aquatic ecological growth of the estuary.

Another adversity of the hyper-turbid regime is the high costs of extensive requirement of dredging. The fairway of the Ems requires high volumes to be dredged throughout the year to maintain a navigational depth (of 10 m) so that the shipyards further up the Ems River remain accessible [van Maren et al., 2015]. The yearly dredging costs of the fairway between Emden and Papenburg are close to 24 million euros [Talke et al., 2007].

However, there is a lack of understanding of the processes that drive the exchange of sediment between the Ems estuary and Ems river, limiting the ability to come up with such targeted solutions that both benefit the local ecology and minimise dredging costs.

1.2 Historical developments in sediment dynamics

The tide in the Ems river has become progressively flood-asymmetric over the past decades due to the anthropogenic activities mentioned previously. This has led to a distinct shift in the dynamics of the sediment regime. The sediment regime keeps itself in hyper-turbid conditions by means of a positive feedback loop involving several sediment dynamic processes driven by tidal asymmetry. Two anthropogenic changes that have changed the tidal asymmetry in the Ems Estuary are dredging and embankment (Talke and De Swart [2006]).

Dredging and embankment both have their implications on the asymmetry of the tidal wave that travels through the estuary. Embankment increases the average depth of the flood tidal wave relatively more than the average depth of the eb tidal wave. This is due to the geometry of the channel (Figure 1.1). When relatively shallow higher located parts of the estuary are embanked, the high water wave does not reach the shallower areas. The low water wave does experience the same effect as the water already does not reach over This radically increases the average depth at high water. Generally, the greater depths correspond to higher propagation speeds of the tidal wave. This, based on the Saint-Venant equations for celerity: $c = \sqrt{gh}$, where h is the water depth and g the gravitational constant. In case of embankment, the propagation speed of the tidal wave its crest speeds up relative to the through. As a result the duration of the rising tide shortens, and the duration of the falling tide lengthens. This makes the tidal wave asymmetric towards flood, having a shorter rising limb and longer falling limb. This shift in asymmetry of the tidal wave means the tidal wave has become more flood dominant. Based on the same principle, dredging increases the depth of the through more than that of the crest. Making the tidal wave more ebb dominant. [Dronkers, 2005]

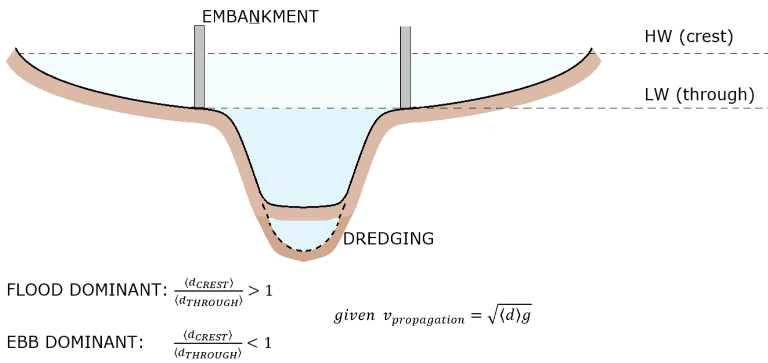

Figure 1.1: *Conceptual model a estuary cross section with average water depths, explaining flood and ebb dominance. From Dronkers [2005]*

The effects of embankment and dredging on the dominance of the tide oppose each other. Embankment makes the tide more flood dominant whereas dredging does the opposite. Talke and De Swart [2006] concluded that the combined effects of dredging and embankment resulted in a more flood dominant tidal wave in the Ems Estuary. In the Emder Fahrwasser - also referred to as the fairway - the tidal wave got more ebb dominant.

The increased tidal asymmetry reinforces the hyperturbid regime in the following way. Flood dominance enhanced the import of fine sediment decreasing the hydraulic drag. This decrease in drag again enhances the propagation speed of the flood tidal wave relative to that of ebb, making the regime even more flood dominant, and in turn more turbid [Talke and De Swart, 2006].

Anthropogenic modifications date all the way back to the 16th century when land reclamation for agriculture started [Compton et al., 2017]. The estuary particularly transitioned to a more turbid state after the decrease of dredging activities in the 1990's and the construction of the weir at Herbrum. The reduced dredging was observed along with a decrease in accommodation space for fine sediment. A smaller accommodation space reduced the Ems its ability to trap sediment, which in turn promotes higher suspended sediment concentrations in the Estuary [van Maren et al., 2015].

To summarise there are three factors that have led to the existing highly turbid sediment regime: 1. the net effect of embankment and dredging resulting in more flood asymmetry 2. a lack of accommodation space for sediment due to embankment, and 3. a decrease in dredging activities which results in less export of sediment out of the estuary.

1.3 Current hypothesis on the hydro- and sediment dynamics at the Geiseleit dam

Van Maren et al. [2021] attempted to identify drivers behind the sediment dynamics at the transition zone from estuary to river. One of the aims of this research was to find out how sediment could travel from the Ems estuary up the fairway into the lower Ems River, even when the tide in the fairway is ebb-dominant, contrasting suggesting sediment transport in the seaward direction. A second aim of the study was to find out what the mechanisms are behind the large dredging volumes that are needed for maintenance of the fairway. Analysis on the EDoM measurement campaign results in the following hypotheses the hydrodynamics and sediment dynamics regarding the mechanisms of up-estuary transport and the need for extensive dredging.
A first hypothesis was that up-estuary transport from the estuary to the Lower Ems river is the result of horizontal flow circulation crossing the Geiseleit Dam and sediment sea-ward flushing by the Ems river. The horizontal flow circulation was assumed to follow the flow from the Dollard over (or through) the Geiseleit dam into the Fairway to Emden and subsequently back to the Dollard via the junction of the Dollard and the fairway (see Figure **??** below).

The flow into the Dollard is flood dominant, meaning that sediment is more advected land inward than outward. Sediment that is advected into the Dollard partly settles on the Geisesteert in front of the Geiseleit Dam. During a subsequent period of flood the sediment can be resuspended by wave action and advected further over the Geiseleit Dam into the fairway. More wave action in the winter leads to more resuspension which strengthens the sediment circulation in the circulation cell around the dam. Calculated sediment settling on the Geisesteert would result in an unrealistic amount of mud accumulation on the Geisesteert suggesting that further advection over the Geissedam must be frequent. However, the episodic character of the remobilization process could not be determined by the EDoM data. When the sediment has entered the the Dollard, a large part of the sediment flows sea-ward advected by ebb flow. However, the analysis of the EdoM measurements found that local flood dominant currents along the southern bank of the fairway drives up-estuary transport. When discharges are higher, this pattern is less clear due to sediment flushing towards the sea [Van Maren et al., 2021]
A second hypothesis that was drawn from the EDoM campaign was that the high maintenance dredging volumes exist (at least partly) due to the sediment flux from the Dollard over the Geiseleit dam, because estuarine circulation driven by salt-fresh water density differences appears insufficient to explain the large dredging requirements. The dredging need was found higher in summer than in winter, which remained unexplained.

The modelling study of Pein et al. [2014] studied the hydrodynamics of residual circulation patterns in the Ems estuary. The vertical profile of the Ems was studied in order to asses the extent to which the (local) hydrodynamics of the estuary can be identified as barotropic or baroclinic. Given this, the study assessed to what extent baroclinicity affects horizontal flow in circulation cells. Baroclinic processes drive flow based

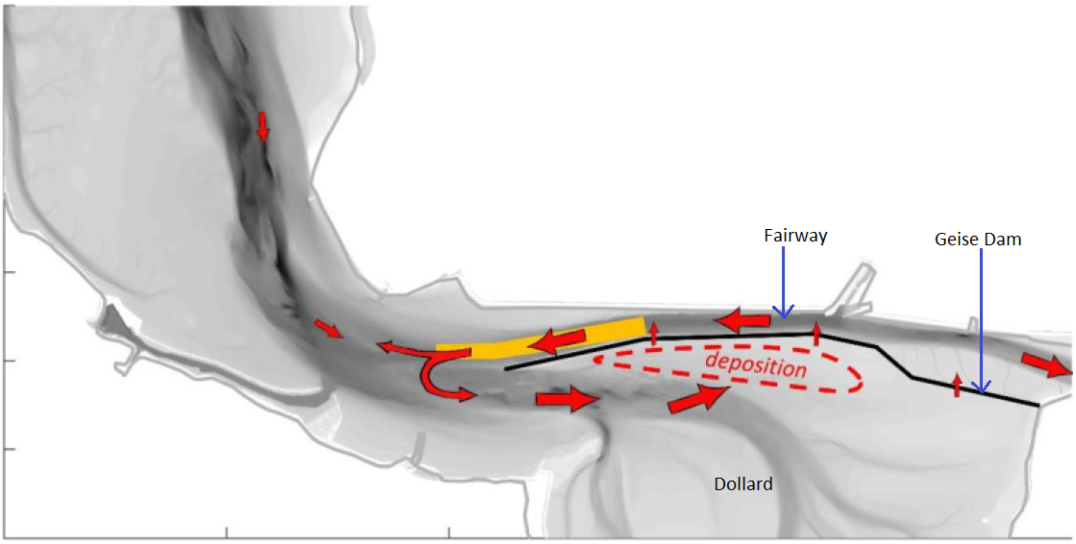

Figure 1.2: Conceptual model of the sediment transport uxes between the Dol- lard and the Fairway to Emden. From Maren et al. [2021].

on pressure gradients from e.g. differences in density from salinity and temperature gradients. Circulation cells were found present in the Outer Ems estuary. The study revealed that a gradient in the vertical density profile could inhibit these horizontal circulation cells. At some places in the outer estuary the tidally-averaged sea-level slope was found very small. At these places baroclinic pressure gradients could exceed the pressure gradients that relate to solely barotropic forcings. The exceedance of the baroclinic pressure gradients over the barotropic pressure gradient reduces the momentum of the horizontal circulation due to buoyancy effects. Baroclinic forcings are less dominant in the study area considered in this Msc thesis. This as density driven flow by differences in fresh and saline water becomes less pronounced upstream of the salinity front which is located just downstream of the Geiseleit dam. In contrast to Van Maren et al. [2021], the study of Pein et al. [2014] only indicates lateral residual circulation cells to be present in the Lower Ems Estuary, and so, it does not indicate a clear residual circulation pattern over the Geiseleit dam. Furthermore, Van Maren et al. [2021] suggests that the hydrodynamics that drive sediment transport over the dam have an episodic character. The question still remains to what extent the circulation over the Geiseleit dam is actually present, and furthermore, what barotropic mechanisms control the episodic character of the flow in this circulation cell.

The hypotheses about the mechanisms driving the net long-term sediment transport (e.g. over a spring neap cycle) such as the existence of a circulation cell, are based on analysis of point observations that do not capture the spatial dynamics of the entire Ems Estuary. Therefore, the indications for the existence of the horizontal circulation cell are apparent, but indirect Van Maren et al. [2021].

A better quantitative understanding on the hydrodynamics in terms of the residual flow patterns and transport between the Ems estuary and the Lower Ems river, will provide progressive insight in the interaction between the mechanisms driving high turbidities and the large required dredging maintenance volumes. Having better insight in the hydrodynamics of the Estuary and the role of the Geiseleit Dam can be used in follow up studies to better quantify long term sediment transport patterns.

1.4 Ocean topography, Eulerian residual return flows, Stokes drift, and tidal Asymmetry

This section provides background theory on the link between residual flows, tidal asymmetry and ocean topography. The term 'ocean topography' is used throughout this thesis to indicate the long-term mean sea water level (MSL). Integrating mass transport over a spring neap cycle at a fixed point in space does not always add up to zero. The residual that remains after integrating over time is what we refer to as residual transport. However,

the term 'residual transport' stands for the flux that is not directly related to forcings by the tidal wave (through flood-ebb asymmetry). The residual transport comes from the total of processes like wind driven flow, river discharge, density driven estuarine circulation and horizontal barotropically driven circulation [Dronkers, 2005]. Surface gravity waves add an excess momentum to the mean flow. This excess momentum is called radiation stress. Radiation stress can lead to an additional mass transport of the water surface layer which is referred to as Stokes' drift [Longuet-Higgins and Stewart, 1962]. In other words, stokes drift is the depth integrated mass transport due to the presence of gravity waves.
The excess momentum, and associated Stokes' drift, is dependent on the direction of the wave propagation. Stokes drift also depends on tidal asymmetry. As mentioned before, tidal asymmetry results from a difference in propagation speed of the trough and crest of the tidal wave, which is influenced by a difference between the depth of the crest and trough of a tidal wave. When a tidal wave is asymmetric, the ratio between the time integrated velocities of the crest with respect to the integrated velocity of the through changes. This means that time integrated surface transport due to the gravity waves (Stokes' drift) also changes [Dronkers, 2005].

The tidal waves induce Stokes drift, which relates to the slow non-zero mass transport resulting from the exertion of gravity waves on the mean flow velocity. Stokes' transport partly contributes to the residual transport which results in a radiation stress gradient. This radiation stress gradient results in a water set-up that can then be counterbalanced by an opposing (residual) Eulerian counter current [Longuet-Higgins and Stewart, 1962]. When stokes drift is counter balanced it flattens the ocean topography [van den Bremer and Breivik, 2018]. Both time integrated Eulerian currents and stokes drift shape the ocean topography. Looking at the agreement in direction of stokes and Eulerian vectors, and comparing this to the ocean topography tells us to what extent the observed time integrated Eulerian vectors are behaving as a residual counter current. An example of this reasoning can be found in Tarya et al. [2010], where time-integrated Eulerian currents where identified as residual counter currents, because stokes and Eulerian vectors were found to oppose each other. Alignment of the vectors would mean that found time integrated Eulerian vectors do not or only marginally counteract water set-up by stokes' drift. In this case the variation in the time averaged ocean topography is enhanced by stokes drift. When vectors are aligned but the ocean topography does not seem altered, residual flow process other than stokes drift are at play. At the Geiseleit dam such a process could the currents driven by radiation stress such as presented in Tarya et al. [2010].

1.5 Research objectives & research questions

The objective for this research is to establish which barotropic tidal mechanisms drive a residual flow circulation at the interface of the Ems estuary and Ems river, and understand to what extent these mechanisms are influenced by the presence of the Geiseleit dam. A process-based numerical model (Delft3D-FM) will be improved and subsequently applied to study the flow patterns around the Geisesteert.

To achieve the research objective, the main research question will be approached through the following subresearch questions:

1. *To what extent is the model capable of reliably reproducing local depth averaged current measurements, gathered at the interface of the Ems Estuary and Ems river?*
2. *How do tidal barotropic mechanisms drive a residual flow in the estuary?*
3. *What is the effect of the Geiseleit Dam on the residual flows?*

The terms 'residual flow' and '(sub-)tidal mechanisms' are defined in Section 2.2.1. In short, residual flow resembles a non net zero mass flow over a certain time period at any given point in space.

2 | Methods

2.1 The Ems-Dollard Measurements Campaign (EDoM)

This study used the flow velocity data from a campaign that is carried out in the Dollard and Ems Fairway near Emden. The measurement campaign consisted of two separate measurement periods. The first period lasted from the 8th of August to the 5th of September 2018. The second measurement period continued from the 9th of January till the 7th of February. Ten locations of stationary flow observations were selected for the purpose of model-data comparison.

At these locations flow velocity profiles were measured with acoustic Doppler current profilers (ADCP), mounted on either mooring chains, bottom mounts, or bottom frames. The mooring chains and bottom mounts were installed by Wasserstraßen- und Schifffahrtsamt Ems-Nordsee (WSA), which is the local German waterway and shipping authority near Emden. Mooring chains were equipped with three Aanderaa Seaguard RCM Multiparameter instruments placed at 1.5 below the water level, 3.5 m above the bottom, and 1.5 meter above the bottom (see Figure 2.1). The multi-parameter instruments all had an ADCP instrument installed. Furthermore, the Bottom frames and bottom mounts were both equipped with upward facing ADCPs.

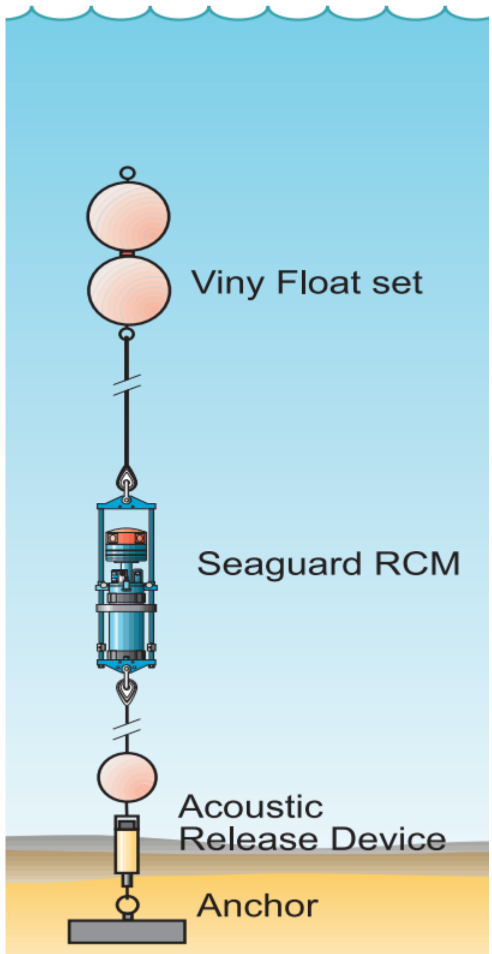

Figure 2.1: *A schematic view of a Aanderaa Seaguard RCM attached to a mooring chain. This instrument was used in the EDOM campaign by the German Waterway and Shipping Authority (WSA).*

Figure 2.1 shows the different measurement locations of the mooring chains (MC), bottom mounts of WSA Emden (BM) and the bottom frames of Rijkswaterstaat (RS).

The difference between a bottom mount and bottom frame is that the bottom mounts were placed by WSA Emden and bottom frames by Rijkswaterstaat. Each of these installations were equiped with a ADCP, either a TRDI WHSC 1200 or Nortek Signature 1000 ADCPs was mounted on the bottom mounts. The type was not explicitly documented per measurement location.

The data of each instrument was averaged over depth as this thesis focuses primarily on identifying residual flows driven by barotropic mechanisms. Each set of instruments had a different amount of depth-bins in which the ADCP data was recorded. Mooring chains had 3 bins according to the three mentioned depths. Bottom mounts had 53 to 66 bins depending the depth that varied with the progression of the tide. Likewise bottom frame data had 20 to 31 data bins. Furthermore, the taken ADCP observations were averaged over 10-minutes, this way they matched the temporal resolution of the model.

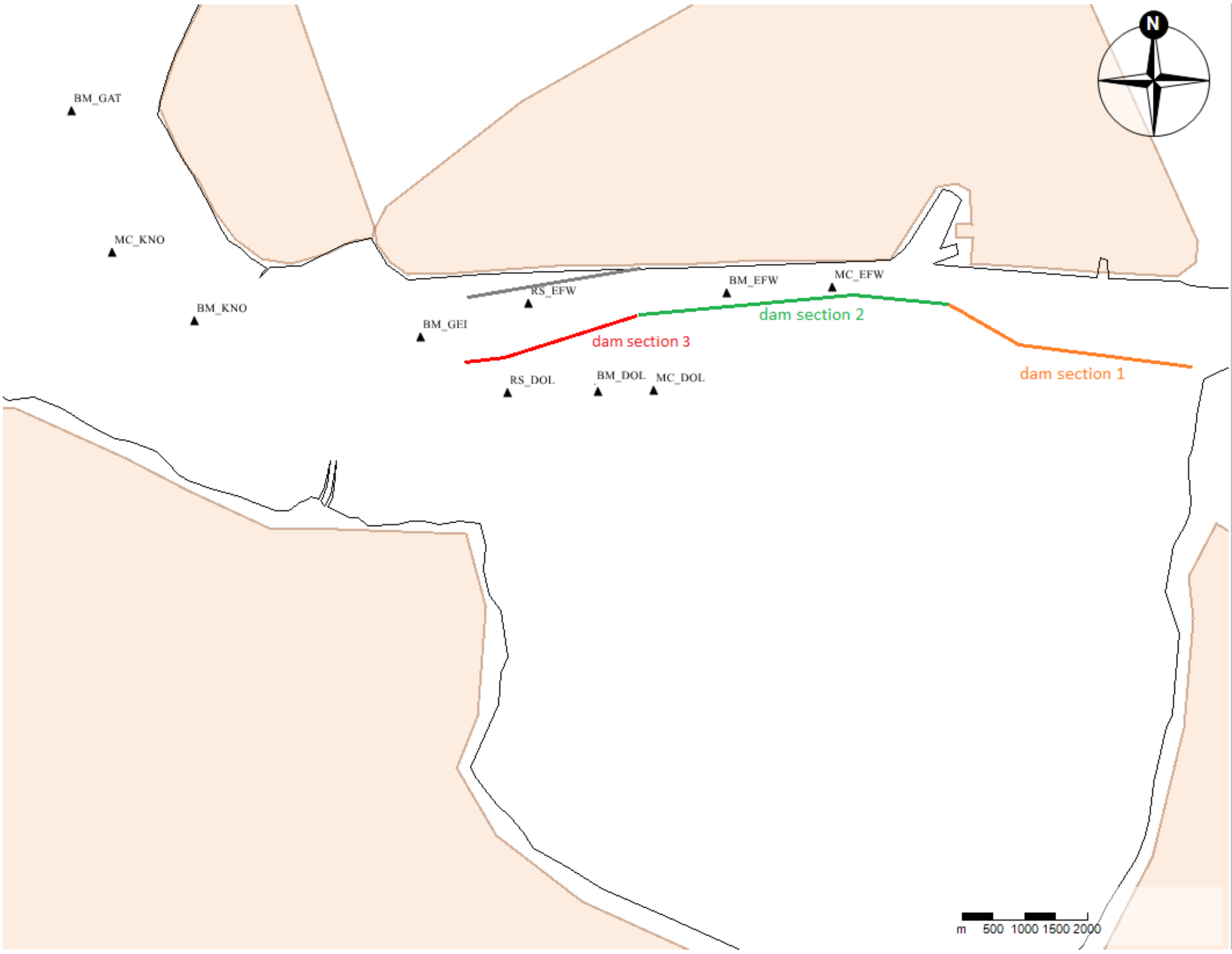

Figure 2.2: *Locations of the EDoM 2018-2019 campaign that were selected for the purpose of data-model comparison. Data is collected at mooring chains (MC), bottom mounts (BC) and bottom frames (RS). The Geiseleit Dam is located between the Dollard and the Emden FahrWasser marked with a coloured line in the center of the map. The red, green, and orange line demarcate the West, Mid, and East dam section respectively.*

2.2 Model setup and scenarios

This study further addresses the hypothesis about the existence of long-term circularly (residual) flow patterns. Numerical modelling is used in combination with the EDoM flow velocity data to: (1) spatially quantify the residual water circulation over the Geisedam and back from the Lower Ems river to the Dollard, (2) identify the main mechanism that drives this residual circulation, (3), provide a better time-integrated estimate of the net residual flow patterns and water mass fluxes, and (4), identify the hydrodynamic effect of the Geiseleit dam on this net residual transport.

2.2.1 Defining residual flow and (sub-)tidal mechanisms

Numerical hydrodynamic modelling was used to improve the insight in spatial patterns of residual flow. The term 'residual flow' is used throughout this thesis, hence it is important to define it well. Residual flow is defined as the non-zero depth average water mass transport over a given time period at any given point in space. The time period used to calculate residual transport in this thesis is 58 M2 cycles. This period is used to capture the non-zero transport induced processes that take place on the time scale of both single tidal waves, and (two) spring neap cycles.

To put the above in perspective, one can imagine that a water parcel is transported back and forth throughout the period of a tidal cycle, then the same mass is transported forward and backward. However, this is not always the case, for example when there is a horizontal water circulation cell. When the depth average flow is rotational over a tidal cycle, the forward and backward tidal mass transport do not cancel each other out, resulting net mass transport. Mechanisms that drive such non-net zero mass transport over time can for example be a result of the local asymmetry of the tidal wave. Other mechanisms are: wind driven flow, river discharge, estuarine circulation and horizontal barotropic circulation.

In this thesis residual mass transport is approximated by calculating velocities. These velocities need to be multiplied with the density of water to get to a one dimensional mass transport. In this thesis, conclusions made about the residual mass transport ignores density difference over space.

Furthemore, this thesis mainly focusses on 'tidal mechanisms'. This term referrers to mechanisms that are directly induced by to the astronomic forcing of the tide. Such as the Stokes drift based on the tidal wave of the M2 constituent. In this thesis a mechanism is called sub-tidal if it is not based on the direct influence of the astronomical tide. So Stokes drift based on wind induced waves would still be considered as a 'sub-tidal mechanism'.

2.2.2 Boundary conditions

The Delft3D-FM model of the Ems estuary was developed by Schrijvershof et al. [2022], and calibrated to realistically simulate tidal wave propagation throughout the estuary. The model was initially set up with the following boundary conditions. At the Western sea side of the model domain, a time-dependent boundary condition for the water level was implemented. These boundary conditions at the sea side exist of two summed forcings, an astronomic component based on 56 tidal constituents, and a non tidal residual (ntr). A separate implementation of these forcings enables the model to simulate with and without the ntr. The ntr is the water level variation that is left after subtraction of the astronomical component. The ntr, also known as 'surge', primarily consists of the meteorologic contribution to the water level [Pugh and Vassie, 1978]. The sea-side boundary conditions were imposed far away from the study area to reduce its direct influence on the model results.

Other implemented time-varying Dirichlet boundary conditions were the river discharges from Westerwolde A and the Ems river. The Westerwolde is a channel that enters the Dollard at its South-East boundary side. Furthermore, a no-flow boundary condition was included at the land border. All boundary conditions above were obtained from Schrijvershof et al. [2022]. This study calibrated the water levels in the model with the Manning roughness. From the Dollard to the western sea boundary a Manning Roughness Coefficient of 0.019 $s/m^{1/3}$ was used. In the upstream direction, onward from the location where the Ems river enters the fairway at Pogum, the Manning roughness was linearly interpolated to a value of 0.011 $s/m^{1/3}$ at Rhede.
As mentioned, this study solely focuses barotropic mechanisms. For this purpose the model is set up with one vertical cell layer producing depth average velocity output.

2.2.3 Model calibration scenarios

Before using the model to gain insight in the hydrodynamics, it was first calibrated. This was done by comparing the model output with the ADCP field data. The model was adjusted in an successive fashion adding a new parameter continuing with the best performing model. In case the model was not improved by the concerning adjustment no adjustment was made. The calibration was performed on depth-averaged flow velocities, adjusting the model by (1) altering the mesh grid resolution around the Geiseleit dam, (2) adjusting the bed roughness, and (3) adding surface advection due to wind. In addition to adjustment three, the model was run with and without the ntr component in the seaside boundary conditions. This was done to analyse to what extent meteorological driven ocean surge affects the model performance. The model configurations simulated for the calibration are summarised in the Table 2.1 shown below.

Wind advection data was obtained from the KNMI High Resolution Limited Area Model (HIRLAM), which was available at the KNMI data platform [Institute].

The various Manning roughness values from Table 2.1 were implemented as uniform value across the estuary, from the Dollard to the sea. In the Ems river, the roughness was interpolated from the uniform value of the Dollard to the same initially used upstream value of 0.019 $s/m^{1/3}$. For the Local grid refinements the accompanying Delft3d software 'RGFGRID' was used. The initial size of the flexible mesh grid cells was about 65 by 180 meters. The fist refinement scenario halves the cells longer longitudinal cell sides. The second refinement

Table 2.1: This table features the for adjusted parameters with the settings used for the model improvement.

	Adjusted parameter	Model settings
1	Bathymetry	2014 (base) 2020 (updated)
2	Manning Roughness $(s/m^{1/3})$	$n = 0.017, 0.019, 0.021,$ $0.023, 0.027, 0.033, 0.033$
3	Local grid resolution	resolution = no refinement $90\text{x}65, 40\text{x}33m$
4	Wind forcing	No wind advection no ntr, No wind advection with ntr, Added wind advection

halves the cells both latitudinal and longitudinally.

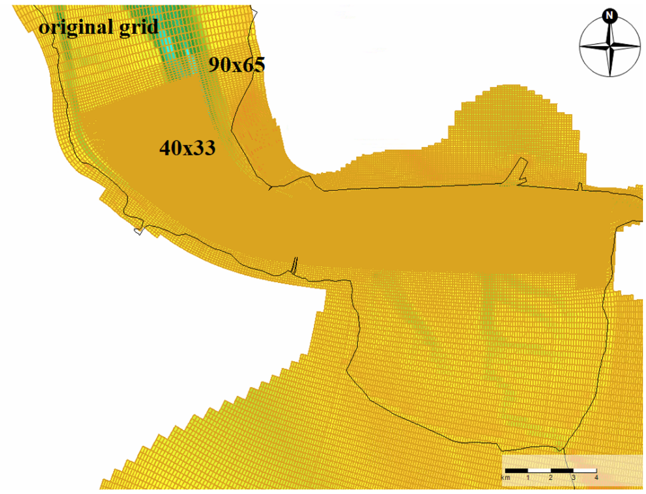

Figure 2.3: *This figure illustrates where the local grid refinements were implemented. The largest grid cells have a resolution of approximately 65 by 180 m whereas the smallest cells were sized 40 by 33 m.*

2.2.4 Modelling dam scenarios

The third research question researches the extent to which the Geiseleit Dam affects hydrodynamics around the Geiseleit dam. For this the same mechanisms as in research question two are used. Using the theory mentioned in the introduction (Section 1.4), an analysis is performed on the interaction between the Geiseleit dam and: the tidal wave propagation and amplification, Stokes transport, Eulerian counter currents and net Lagrangian transport. The tidal wave propagation and amplification was analysed through plotting a map of the tidal phase and tidal range. The phase and tidal range were obtained by performing an online Fourier analysis. Using Delft3d its web-based analysis minimized the the calculate time.

Four different Dam scenarios were modelled. The Dam was implemented in Delft3d-FM by means of implementing a weir, because it allows for variations in height. Three different dam heights were implemented: 0.0 m, 0.5 m and 1.0 m. A fourth scenario was to implement an impermeable dam. The implemented model bathymetry only includes the sand plates that have been formed around the current dam, and not the dam itself. The actual dam is too thin compared to the spatial resolution of the bathymetry data set, and is there for heavily smoothed out. Consequently, it was assumed that no dam was present in the bathymetry. This then implies that the weir heights were added on top of the sand plates present in the bathymetry data set.

2.3 Processing and Analysis

A data analysis that was used for the calibration of the model. This data mainly consisted of a comparison between the model results and the EDoM field data. Before the model-data comparison could be made, a number of steps were taken to make the data comparable. These steps will be elaborated in the following section. Moreover, two metrics were chosen to quantify the performance of the different model adjustments. Furthermore, this sub-chapter elaborates on the use of these metrics, and comments the choice for these metrics.

2.3.1 Approach of the calibration process

The model adjustments were made in a consecutive fashion. An adjustment was made to the model after which the model performance was measured, next, the best model configuration was used for the next run. This consecutive way of adding parameters and measuring the model performance does not take into account possible synergistic or antagonistic effects due to possible parameter dependence. This method of calibration measures the overall improvement due to the addition of a parameter, but it does not measure the independent additive contribution of each parameter. Insights in the independent parameter statistics could be made by using a variance-co-variance matrix such as described by Hill [2000]. Only this requires the modelling of all possible parameter configurations. The choice was made to calibrate the model consecutive fashion due to time constraints, and the underlying idea that the overall model performance is of primary concern.

2.3.2 Statistical Metrics

The model performance was quantified through the use of two statistical metrics, the model skill-score (SS) and the root mean squared error (RMSE). These two different metrics were chosen because they allow for a standardised and equal-unit interpretation of the prediction error. The SS serves to get a better overall unitless indication of the model performance. This as the SS metric standardises the summed squared error (SSE) for location-specific magnitudinal differences in the prediction error of the flow velocity. In contrast, the RMSE provides insight in the magnitude of the prediction error in the same unit as the flow velocity .

The RMSE is a commonly used statistic that provides an actual unit indication of the difference between two datasets [Ji and Gallo, 2006], in this case this concerns the model output and the observation ADCP data. For the Skill Score the definition of Willmott [1981] was used. This metric has been broadly applied among studies in the field of coastal hydrodynamic and sediment morphological modelling. Examples of its use are found in studies such as that of Tarya et al. [2010] [Li et al., 2005] [Warner et al., 2005], and in more recent work such as [Rathod and Manekar, 2022] [Wang and Pan, 2018]. Equation 2.2 below was used for skill score calculations in Matlab:

$$SS = 1 - \frac{Summed\,Squared\,Error}{Potential\,Error} \tag{2.1}$$

which can also be expressed as:

$$SS = 1 - \frac{\sum_{N}^{i=1} |X_{mod} - X_{obs}|^2}{\sum_{N}^{i=1} (|X_{obs} - \bar{X}_{obs}| + |X_{mod} - \bar{X}_{obs}|)^2} \tag{2.2}$$

Here X is the eulerian flow velocity, N is the number of time steps of the model run, and $\overline{X}$ is the time averaged flow velocity. Tarya et al. [2010] As can be seen in the equation 2.1 above, the skill score is the ratio between the summed squared error (SSE) and the potential error. The potential error is a total of, the variance between the model and the observations, and the variance within solely the observations. The SSE is standardized as the the potential error depends on the *range* of the observation and model time-series. [Ji and Gallo, 2006]

The skill score varies between 1 and 0. A value of 1 indicates perfect agreement between the model SSE and the potential error.

In order to summarise the model performance for all the measurement locations, the metric outcomes were averaged over the ten locations.

2.3.3 Pre-processing of the calibration data

In the calibration and model improvement phase of this thesis, Matlab was used to compare observed and modelled flow velocity data. The model flow velocity time-series were compared at each of the measurement locations of the Edom campaign (see Figure 2.2). The purpose of this comparison was to analyse the model performance through the use of the statistical metrics explained in the previous section. The metric could not be implemented straight away however. A few pre-processing steps were performed to make the model and observation data comparable.

This study focusses on *barotropic* hydrodynamic processes. For this reason, the Delft3D-FM model was set-up in such a way that it already produces depth-averaged eulerian flow velocities. Yet, the ADCP observation data was delivered in separate depth bins. Therefore, the first pre-processing step was to take the depth average of the observation data. This, through taking the simple average of the different depth bins.

The second performed pre-processing step was to flip the phases of some of the ADCP-time series. When the modelled and observed timeseries were plotted and compared, some of the observed series turned out to be 180 degrees out of phase. This was likely due to deviating axis definitions of the ADCP measurement instruments. The North-South velocity vector components were flipped of stations RS-DOL and RS-EFW. (See Figure 2.2)

The modelled and observed flow velocities were initially described in terms of a North-South and a East-West velocity component.

As a third pre-processing step, these components were transformed to components in the primary and secondary flow direction. The primary and secondary flow direction is often also referred to as the stream-wise and stream cross flow direction. The stream-cross and -wise flow directions are defined as the direction in which the

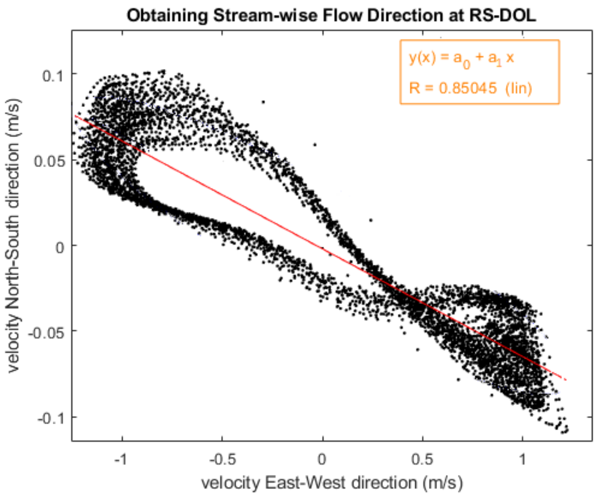

Figure 2.4: *An example of observation velocity data through which and a line is fitted to obtain the stream-wise and cross flow direction. The red line gives the fitted stream wise axis.*

average Eulerian flow velocity is greatest and smallest respectively.

This definition can be visualised with a tidal ellipse. A tidal ellipse is formed as a result of the in and outward propagation of the tidal wave. When the tide propagates back and forth through the estuary, the movement of a water a particle does not move in a straight line per se. For that reason, an ellipse is formed when plotting the Northern, against the Southern velocity component. Figure 2.4 provides an example of a fitted tidal ellipse in blue. The stream wise and cross directions are defined along semi-major and semi-minor axis of the ellipse.

In fact, the north and south velocity components of both the model and the observation data did not form an ellipse at all of the measurement locations. In such cases ∞-shapes were formed. (see scatter points in Figure 2.4) As a consequence, determining stream cross and wise directions was not possible based on fitting an ellipse by means of the renown 'fitellipse' package of Matlab. Alternatively, the Matlab package 'StreamAndCross' from Open Earth Tools was used. This package uses simple line fitting as illustrated by the orange line in Figure 2.4.

The fourth pre-processing step was to compensate for one hour of phase difference between the modelled and observed velocity time-series. A consistent one hour disagreement in phase was found, due to a winter-summer time difference between the model and the measurements. The the model modelled in GMT while the measurements were likely in GMT+1. However this difference could not be confirmed as no GMT reference was made in the documentation of the EDom campaign. ([Mol, 2018, Wunsche, 2019, Becker, 2018])

The final pre-processing step was to cut the modelled and observed velocity time-series to the time domain at which both model and observed data was available. Cropping of the time-series was done for each measurement location, as each location had a different time overlap with the model output.
Not all measurement locations had equal start and end times, nor did they have the same duration. The measurement durations of the 2018 data set varied from 20 days at RS-EFW up to 28 days at BM-DOL. Moreover, starting dates maximally differed with 17 days resulting in a cross-locational time domain overlab of only 11 days. The available observations outside this 11-day time span were used to extend the calibration period. ([Mol, 2018, Wunsche, 2019, Becker, 2018])

2.3.4 Model integration of non tidal residual flow

A harmonic analysis was performed to asses how well the non-tidal residual flows (ntr) are integrated in the model. Ntr time-series for each measurement location were obtained by subtracting the harmonic velocity signal from the original signal (see Figure 3.3). The harmonic velocity signal was obtained by performing a Fast Fourier transform with a tool called T-TIDE. T-TIDE is a widely used Matlab package used among oceanographers [Pawlowicz et al., 2002]. This package was for also used in the reference study of Tarya et al. [2010] on residual transport patterns and the role of the barrier reefs.

2.3.5 Validation of tidal wave propagation

One of the hypotheses studied in this thesis is that there is a residual water circulation over the Geiseleit dam. A driving mechanism behind this could be the way in which the Geiseleit dam alters the respective along-dam propagation of the tidal wave at the Northern and Southern side of the dam. A relative difference in the Northern and Southern tidal propagation could result in a net water-level gradient over the period of a tidal wave.

The extent to which this mechanism can be modelled accurately was assessed by looking for phase differences between the modelled and observed propagation velocity of the tidal wave. The phase shift between the modelled and observed tidal wave propagation was obtained by calculating the difference in the timing of the velocity maxima and minima present in the stream wise velocity time series. This was done for every measurement location indicated in figure 2.2. A map was made indicating the phase difference at each location.

The uncertainty in the the position of the tidal wave North and South of the dam, was quantified by calculating the Mean error (ME) in timing of the max flood and ebb stage of the tidal wave. The use of the max flood and max eb stage provides a clear reference of the stage of the tidal propagation. Though observing this reference at measuring points North and South of the dam, the difference in timing of between timing of tidal wave northern and southern side was calculated.

The timing of the max flood and max ebb stage was obtained through identifying the local maxima and minima in the stream wise velocity time-series. The timing of the velocity maxima were found by means of the Matlab function 'findpeaks'. This function only obtains maxima, therefor the timing of velocity minima were obtained by inverting the velocity signal.

Validation of the tidal wave propagation was necessary because too large uncertainty in the relative position between the tidal wave North and Southern of the dam, can lead to inaccurate modelling of the mean water level gradient over the dam. Moreover, uncertainty in this relative position could result in a North-South flipped water level gradient. This could in turn false conclusions about the direction of a residual circulation pattern. This could for example happen when the tidal wave travels much slower into Dollard (South) than it actually does. In this case the tidal wave North of the dam is propagates ahead of the wave at the Southern side, falsely resulting in inverted water level gradient across the dam.

When the velocity time series have dissimilar timings North and South of the dam, the tidal wave at one side of the dam has already propagated further relative to the other. The Mean Error time error of the max was calculated

The modelled tidal propagation velocity difference between the tidal wave propagating North and South of the Geiseleit dam should be small enough to not to let the gradient over the dam invert. The more certain the propagation velocities at the north and south of the dam, the more reliable the relative propagation difference in velocity between the north and South of the dam. Section 3.1.3 elaborates on how much uncertainty is acceptable with regard to gradient inversion.

2.3.6 Analysis of amplitude and Phase

The propagation of the tide was analysed performing a Fast Fourier transform (FFT) on the simulated water level data. The FFT was used to obtain the amplitude and phase of the M_2 tidal height component, over a period of two spring-neap cycles. A fast Fourier transform is the same as a normal Fourier transform except for the fact it uses a discreet set of frequencies. The frequency of a total of 58 cycles of the M_2 tidal constituent was used (corresponding to the two spring-neap cycles).

This analysis was performed by using the build-in online data processing service of Delft3D-FM. The service was automatically accessed by the inclusion of Fou-files in the model directory.

2.3.7 Mean Eulerian, Stokes Drift Lagrangian velocity calculations

Research question two focuses on gaining insight in what hydrodynamic mechanisms drive a Stokes transport was calculated in order to gain insight in the extent to which tidal wave action plays a role in the residual mass transport.
Mean Stokes transport was calculated over a period of 30.02 days, equalling two spring-neap periods and 58 periods of the M_2 tidal constituent.

First order estimates of the mean stokes velocity vectors were calculated based on the definition presented in [Longuet-Higgins and Stewart, 1962]. This formulation was later used and reformulated for calculation of northward and southward velocity components in Tarya et al. [2010], Wei et al. [2004]

According to Tarya et al. [2010] the North-South (Vs) and East-West (Us) stokes velocity vector components were expressed by the equations:

$$U_s = \frac{1}{H}\left[\langle U\zeta\rangle - \frac{\partial}{\partial y}\left\langle HU\int V dt\right\rangle\right] \tag{2.3}$$

$$V_s = \frac{1}{H}\left[\langle U\zeta\rangle + \frac{\partial}{\partial x}\left\langle HU\int V dt\right\rangle\right] \tag{2.4}$$

These equations provides the Stokes velocity vector component for any given point in space. In this study these equations had to be implemented on Delft3D-FM its irregular grid. The equations above were implemented in Matlab as demonstrated in equations 2.5 and 2.6 below.

$$U_s = \frac{1}{H}\left[\langle U\zeta\rangle - \frac{\partial}{\partial y}\left(\langle\zeta U\rangle \odot \int_{t=t_{start}}^{t=t_{start+30.02days}} V dt\right)\right] \tag{2.5}$$

$$V_s = \frac{1}{H}\left[\langle U\zeta\rangle + \frac{\partial}{\partial x}\left(\langle\zeta U\rangle \odot \int_{t=t_{start}}^{t=t_{start+30.02days}} V dt\right)\right] \tag{2.6}$$

Here, the $\odot$ operator represents an element-wise grid cell multiplication. An element wise multiplication means a multiplication in which the value of one parameter is multiplied with the value of another according to their matching Delft3D-FM mesh cell. Furthermore, ζ stands for the instantaneous water depth at each grid-cell and H is the time-averaged water depth. U and V are the northward and Eastward Eulerian velocity components. The angle brackets are used to indicate the that the time-average is taken over two spring-neap cycles. The same two spring-neap cycles were also used as limits of the integrant that aggregates U and V.

2.3.8 Interpolation for Stokes calculations

In Equation 2.5 and Equation 2.6, $\frac{\partial}{\partial y}$ And $\frac{\partial}{\partial y}$ signify a spatial gradient with x defined positive in the Eastward direction and y is defined positive in the northward direction. Due to Delft3D-FM its irregularly structured grid the spatial gradient could not be calculated by simply using the values of neighbouring cells. This, as the cell centres of the neighbouring cells were not structured in a neatly aligned Cartesian grid. Therefore the term within the round brackets was first interpolated to a regular grid using linear interpolation.

Ideally, the U, V and ζ parameters would have been equally interpolated in order to keep them the same as the ones used within the round brackets. However, Interpolation of $U\zeta$ at every time step turned out to be too computationally expensive. Therefore the choice was made to only interpolate time-averaged terms. Meaning that the U, V and ζ outside the round brackets were first time-averaged and then interpolated, instead of the other way around like performed for the parameters within the round brackets. The interpolated values were re-sampled to a much higher resolution regular grid to marginalise the interpolation error between the U, V and ζ terms in and outside the round brackets. The resolution of the regular grid was about nine times as small as the original grid.

The interpolation on a regular grid caused values to be present on land masses also. These invalid values were filtered out by means of the Matlab function 'Inpolygon' in combination land-boundaries retrieved from the model.

3 | Results

3.1 Model Calibration

3.1.1 Effect of model adjustments

Figure 3.1 contains target plots that present the model output improvement of the Eulerian flow velocities at each of the ten measurement locations. The scatter points in the target plots show the ensemble mean model performance of all the measurement locations due to a certain model adjustment. The different model adjustments are mentioned in Table 2.1. Appendix A.2 contains target plots in which the performance of each measurement location is shown separately.

The target plots show the model performance in terms of the Root mean square error (RMSE) and skill Skill score (SS). The model has improved when a model adjustments results in an increase in the SS. The opposite is true for the RMSE, here, the model improves when the RMSE gets smaller.

For each model adjustment two plots are made, the top one describing the improvement in the stream-wise direction, and the bottom one describing the improvement in the stream-cross direction. Within each target plot the distinction is made between the improvement in a 'tidal' (green) and 'non-tidal' signal (blue). The 'tidal' signal gives the model improvement of the signal that includes both a tidal component and a non-tidal residual (ntr), based on the harmonic analysis explained in 2.3.4. The 'non-tidal' signal only includes the ntr.

A couple remarks can be made based on the observed improvement of the 'tidal' and 'non-tidal' flow velocity signals.

A first observation was that when adding a tidal harmonic component to the model, the model performs increasingly well. The combined performance of the ntr and tidal component is greater than the sum of the separate performance of the ntr and tidal components. In other words, their combined effect is synergistic. This stresses the relative importance of the tidal harmonic velocity component over the ntr velocity component to the model performance.

Secondly, even though the model generally simulates the 'non-tidal' signal worse than the 'tidal' signal, the ntr was still modelled moderately well in the stream wise direction. In this direction, the ntr of the best model run reached a skill score of 0.93. The corresponding RMSE of 0,09 m/s was high in comparison to the amplitude of the ntr signal. The amplitude of the residual velocities signal was found to be in the order of 0.35 m/s at most measurement locations. A good skill score and worse RMSE indicates that the order of magnitude is modelled well but the timing less. An example of this can be seen in figure 3.3. The plotted RMSE values of the 'tidal' signal are in fact much better compared to that of the 'non-tidal' values. This, as the average amplitude of the 'tidal' signal is much larger, more in the order of 1.5 m/s. (see left stream wise velocity plots of Figure 3.2)

Overall, Figure 3.1 clearly shows that the modelling of Eulerian flow velocity in the stream wise direction are modelled with high performance scores, whereas flow velocities in the stream cross direction are with lower scores. For further modelling the stream cross velocities were not further improved, as accurate modelling of the flow velocities in the stream-wise direction is most important to model the tidal propagation.

The target plots show that model improvement was achieved by adjusting the Manning Roughness Coefficient. For further modelling a Manning Roughness of 0.023 $s/m^{1/3}$ was used, as this value gave the best model result. The second adjustment that most influenced results was updating the bathymetry. In contrast, making local grid refinements in the Dollard and the Emden Fahrwasser only yielded a marginal improvement. For further use of the model no grid refinements were implemented, considering that local refinements to resolutions of 90x65 and 45x33 meter resulted in a significantly longer calculation time. Similarly, the inclusion of wind advection onto water surface of modelling domain also resulted in a marginal model improvement. Despite this, wind advection was still included for further modelling as it did not majorly increased the calculation time.

The target plot featuring the wind advection, see Figure 3.1 d, also includes a scenario in which the water level boundary condition was changed. As mentioned in 2.2.2, these model boundary conditions are set up in such a way that the model can be run without the ntr contributing to the water levels. The scatter points market as 'only tidal bc' illustrates the perfomance of a modelling scenario in which no ntr was included as part of the boundary conditions at the ocean side. The scatter

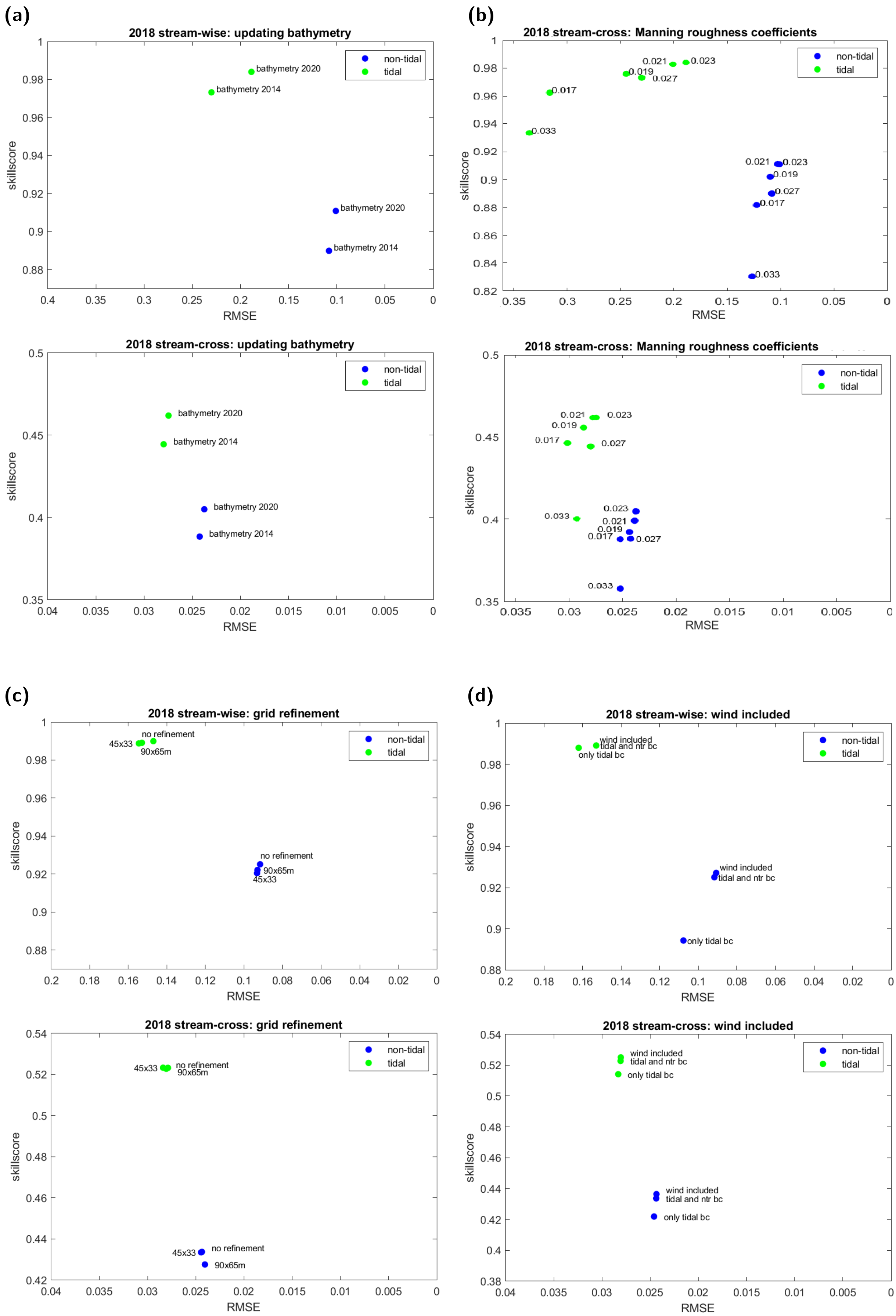

Figure 3.1: *Target plots showing model performance. These plot show of the Skill-score (y-axis) against RMSE of modelled versus observed depth-averaged flow velocities (x-axis). One dot in the plot features the mean RMSE and Skill score value of all the observation locations. Target plot 1a and 1b show the effect of updating the bathymetry. Plot 2a and 2b show the effect of updating the roughness. Plot 3a and 3b show the effect of different the grid resolutions. 4a And 4b show the effect of including wind in to the model. 'a' Provides the model performance along the major axis and 'b' along the minor.*

points market as 'tidal and ntr bc' gives the performance of a model scenario that includes *both* the contribution of the ntr *and* tidal constituents.

The addition of the ntr component to the boundary conditions does not seem critical to the model performance. This as this addition only yields Skill Score increase of 0.02 and an negligible increase in the RMSE of 0.0001 m/s. The addtion of wind advection within the boundaries of the model does not further increase the model input either.

Figure 3.2 shows an example of how one single velocity series has improved from before to after being the calibration was performed. For this, the time series at RS-DOL was used (see 2.1) as an example. The taken example representative for the improvements achieved. The plots show velocity time series extending over two tidal waves. The modelled Eulerian velocity time series is given in blue, and the observed time series in orange. At the top of the plots, the two model performance scores are given of the *entire* time series.

From the time series can be observed that the calibration improved both the phase and amplitude of the modelled velocities. Improvements were observed across all locations and across the entire time domain. The initial phase difference can be seen in the top-right figure. Here, the modelled blue line is off by about 1 to 1.5 hours compared to the observed orange line. The phase difference was not consistent over time and space. The improvement of the phase meant that blue line moved forward as well as backward in time, fitting the observed line better overall. Regarding the amplitude, the modelled peaks overlapped better with that of the observed across all locations and across time.

With regard to the stream-wise velocities, the improvement of the phase was especially seen back in the RMSE. The average RMSE improved from 0.25 m/s before calibration to 0.15 m/s after calibraion. This is a moderate improvement considering that most series had a average max flow velocity of 1.5.

3.1.2 Non-tidal residual

Part of this research is to find out to what extent the flow around the Geiseleit dam is driven by sub-tidal or tidal hydrodynamic mechanisms. Figure 3.3 shows the result of the performed harmonic analysis (see Section 2.3.4) at a single measurement location RS-DOL. This point serves as example for the other meassuring points.

Figure 3.3a, shows a comparison between the observed Eulerian velocity and the corresponding harmonic velocity over time. Figure 3.3b, shows a comparison between the modelled harmonic velocity time series - obtained from the harmonic analysis - and the *observed* velocity time series.

Figure 3.3 (a) essentially shows that the tidal harmonic signal describes a large part of the total observed velocity signal. This because, the purely tidal - or harmonic signal - matches the observed signal well. This was also the case for other measuring points. Here the harmonic velocity time series was also very similar compared to that of the non-modified Eulerian. Figure 3.3 (b) shows a difference in the model and observation - based harmonic velocity signal. This difference can be largely explained by the fact that, the non-modified modelled and observed Eulerian signal are dissimilar. Input for the harmonic analysis logically also leads to a difference in the harmonic. is different.

As described, the ntr was calculated by subtraction of the harmonic signal from the total signal. The ntr is shown in Figure 3.3c. At most measurement locations was observed that the velocities of the ntr ranged in the same order of magnitude such as seen in plot (c). Despite this, the peaks of the ntr signals were not well modelled. The model especially failed to accurately reproduce observed the peaks as it often overshoots them such as can be seen at 18:00 in Figure 3.3c. The model modelled a the timing of the peaks fairly well, however this statement is only based on a visual observations of the series at each measuring location.

3.1.3 Validation of tidal wave propagation with in-situ data

Figure 3.4 shows the result of the velocity phase analysis as according section 2.3.5.

The model Skill Score respectively improved from 0.97 to 0.99 from before to after calibration. Based on solely the Skill Score, the performance seemed already sufficient. However not having a very well modelled velocity phase would still be problematic for testing the hypothesis of water circulation over the Geiseleit dam as explained in section 2.3.5.

In order to still be able to make supportable comments on the direction of residual circulation over the Geiseleit Dam, the time placement of the velocity minima and maxima was analysed. The velocity minima indicates the max ebb phase of the tidal wave, and the

(a) Before Calibration

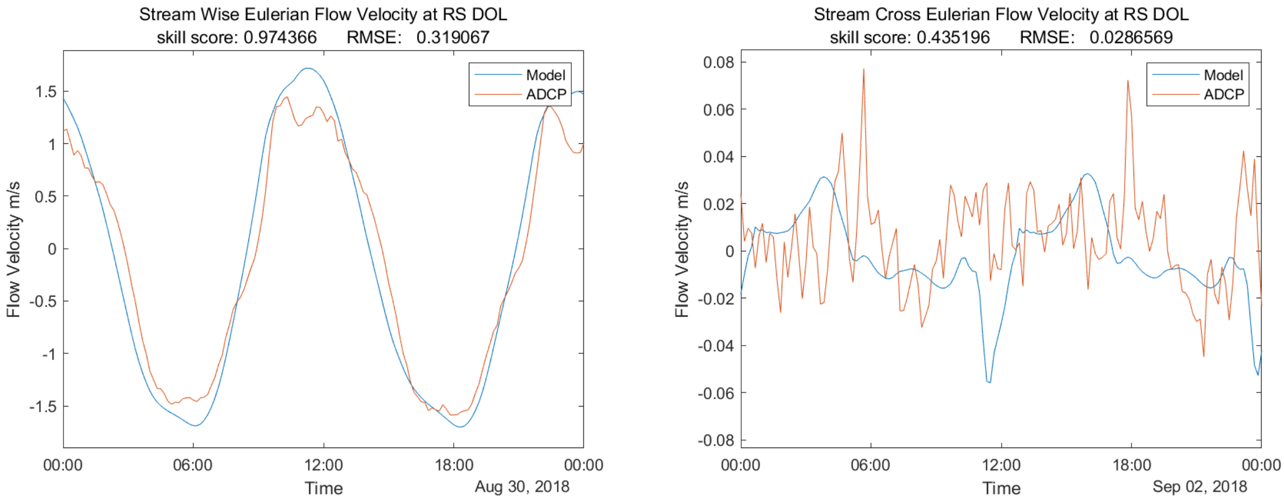

(b) After Calibration

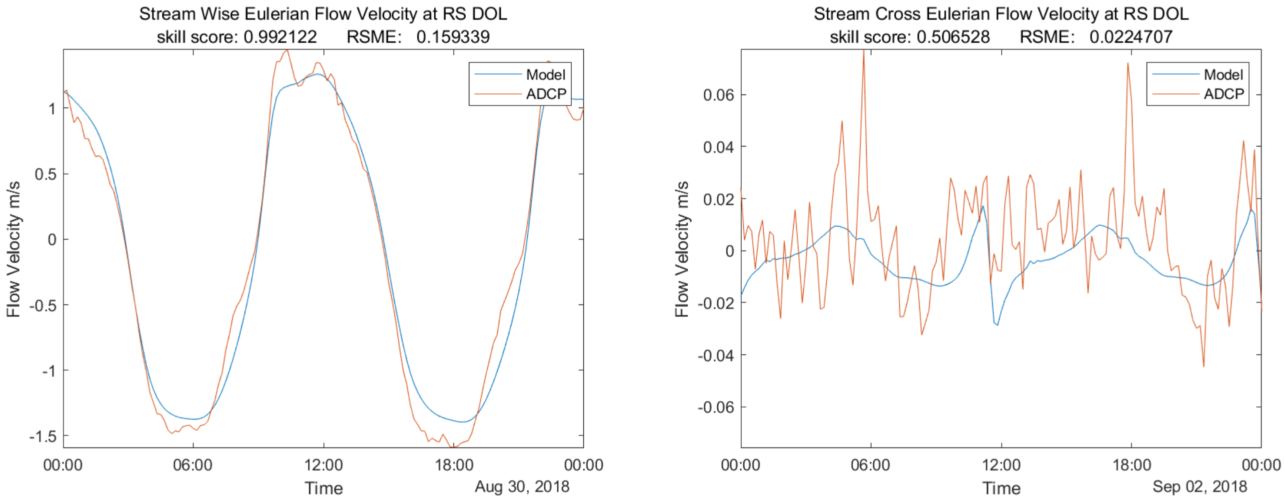

Figure 3.2: *Figure A above shows a data- model comparison of the Eulerian flow velocity over time. The upper two figures show a comparison before the calibration, and the lower two figures show a comparison after the calibration. This series is measured and modelled at measuring point RS-DOL, located near the entrance of the Dollard. The left figure shows the flow velocity along the major tidal axis against time. The figure on the right displays the flow velocity along the minor tidal axis.*

maxima indicate the max flood phase of the tidal wave. This wave the velocity peaks and minima serve as a reference phase through which the position of the tidal wave North and South of the dam can be compared.

The average time difference between modelled and observed velocity extremes (see 3.4), indicate extend of uncertainty in the position of tidal wave along the Geiseleit dam. The left map shows the average time difference between the timing of the modelled and observed velocity maxima at every measurement location. The colours indicate the mean error (ME) of the timing of the max ebb tide in minutes. The right map shows the same but then for the velocity minima. Here, the colours indicate the mean error in timing of the max flood tide.

The difference in the ME of the max *flood* timing, between the North and South seems to be between 5 and 10 minutes (left plot in Figure 3.4). In contrast, a greater difference in the ME of the max *eb* timing was observed. Here, the difference in the ME North and South of the dam seems range from 5 to 25 minutes (see left plot in Figure 3.4).

The max flood tide and max ebb tide have an acceptable phase shift when the waves are respectively 900 meter and 2250 meter apart. At these distances two points with same phase of the tidal wave, north and south of the dam, are less likely to overlap and thus

(a)

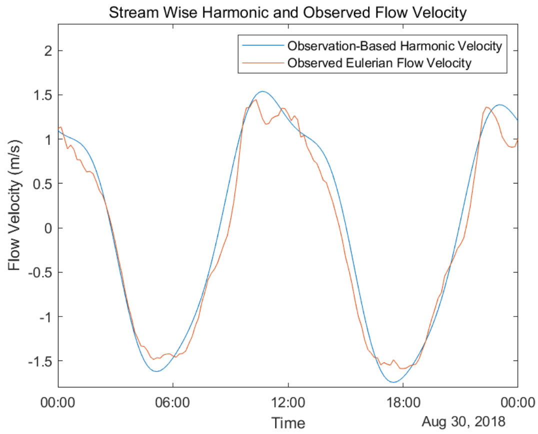

(b)

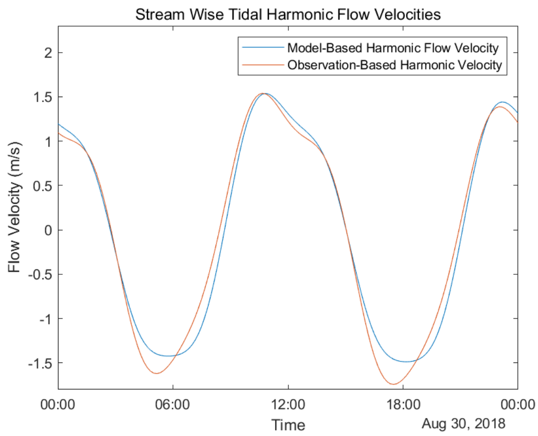

(c)

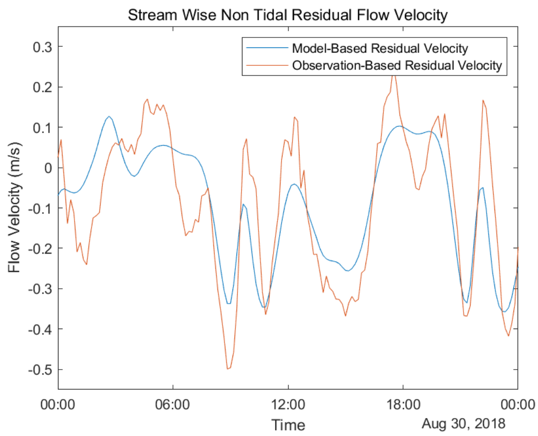

Figure 3.3: *The three plots above show comparisons of exemplary output velocity time series resulting from the harmonic analysis. These time series were obtained after calibration from the location RS-DOL. Figure A shows a comparison between the observed Eulerian flow velocity and the corresponding harmonic Eulerian velocity over time. Figure B shows the Harmonic Eulerian flow velocity against time at the same location. An harmonic flow velocity signal was obtained though performing a tidal harmonic analyses. The figure on the right hand side displays the residual Eulerian flow velocity over time at the same location. Both the left and right plot display velocities projected along the major flow axis. These plots display the harmonic residual Eulerian time series of the best model run obtained after calibration.*

cause a north-south flip of the water level gradient. The values above are based on the following reasoning. Regarding peaks: multiplying the mean error of max 10 minutes with and average propagation velocity of 0.75 m/s the approximate distance that two waves should be apart is 900 meter. This also includes a multiplication by 2 as two tidal waves are considered. similarly regarding velocity minima: a mean error of max 25 minutes and an average propagation velocity of 0.75 m/s yields 2250 meter. The concept above is sketched in Figure 3.5 below.

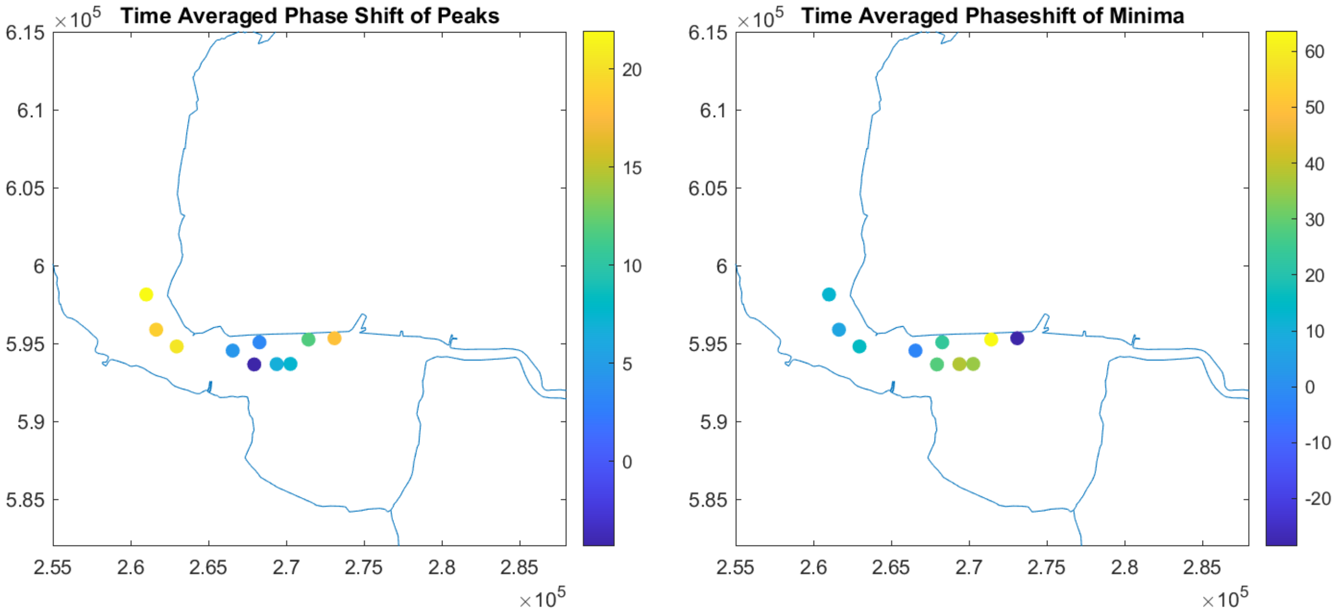

Figure 3.4: *The figure above shows a map of mean phase differences between the model and the observation data after calibration. The left map shows the phase difference of high tide peaks, and the right displays the phase difference of low tide minima. The average phase difference is based on the different placements of the harmonic peaks in time.*

3.2 Tidal Propagation Patterns

Figure 3.6 shows the modelled phase and amplitude of the M2 constituent during spring and neap tide. This, based on the Fast Fourier Transform of Section **??** and the reference model scenario with a dam height of 0.5m. The figure shows a slight gradual increase in amplitude of the M2 tide in the Eastward direction. The Geiseleit Dam seems to induce more amplification of the M2 tide in the fairway - North of the dam - compared to in the Dollard. There is a difference in amplification in the range of 1-2 cm/s during both the spring and neap tide. This compares to a modelled overall tidal amplification of about 9 cm/s during spring and 4 cm/s during neap tide, from the location of BM-GAT to the Dollard near Emden.

A pattern of Eastward amplification is most visible during the neap tide. The top left map in figure 3.6, shows how there is equal amplification at the western front of the dam (in yellow). Heading in Eastward direction along the dam, there is an increasing cross-dam difference in tidal amplification. For both neap and spring tides the tidal amplification lessens towards the South-East end of the Dollard, which can likely be attributed to shallowing. Moreover, a decrease amplification is observed near the at the end of the Fairway at the entrance of the Lower Ems river. Tidal amplification increases again upsteam of the entrance during both spring and neap tides.

The Cophase colour maps show that the M2 tide propagates perdominantly along the dam.(see right-hand plots of Figure 3.6) In the Dollard, the M2 tide follows the bathymetry deflecting to the South East. The Figure clearly shows how the celerity of the tidal wave propagation in higher in the Dollard than in the Fairway. This as the colour gradient shown in the phase plot at the North side of the dam is more stretched out compared that of the South. Cross-dam difference in phase speed can be attributed to the presence of the dam as the location of the dam well coincides with the line at which a sharp phase shift occurs.

Moreover, the M2 phase speed decreases in the upstream direction as the colour gradient gets larger. This observation of decreased phase speeds matches what was observed in the ADCP measurements. A propagation velocity decrease of 10% during neap and 15% during spring tide was observed from the location 'BM-KNO', a observation point just west of the dam, to 'MC-DOL', a point South of the dam. Similarly, a decrease of about 30% during neap and 45% during spring tide was observed from 'BM-KNO' to 'BM-EFW' North of the dam. The tidal wave in the Fairway slows about 20%

(a)

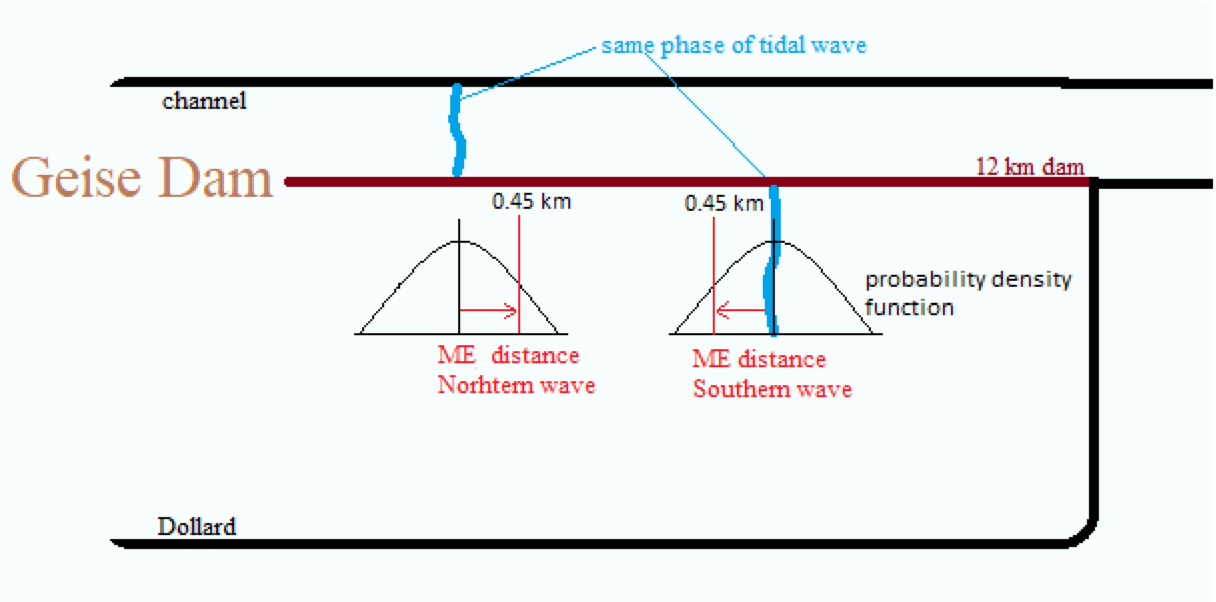

(b)

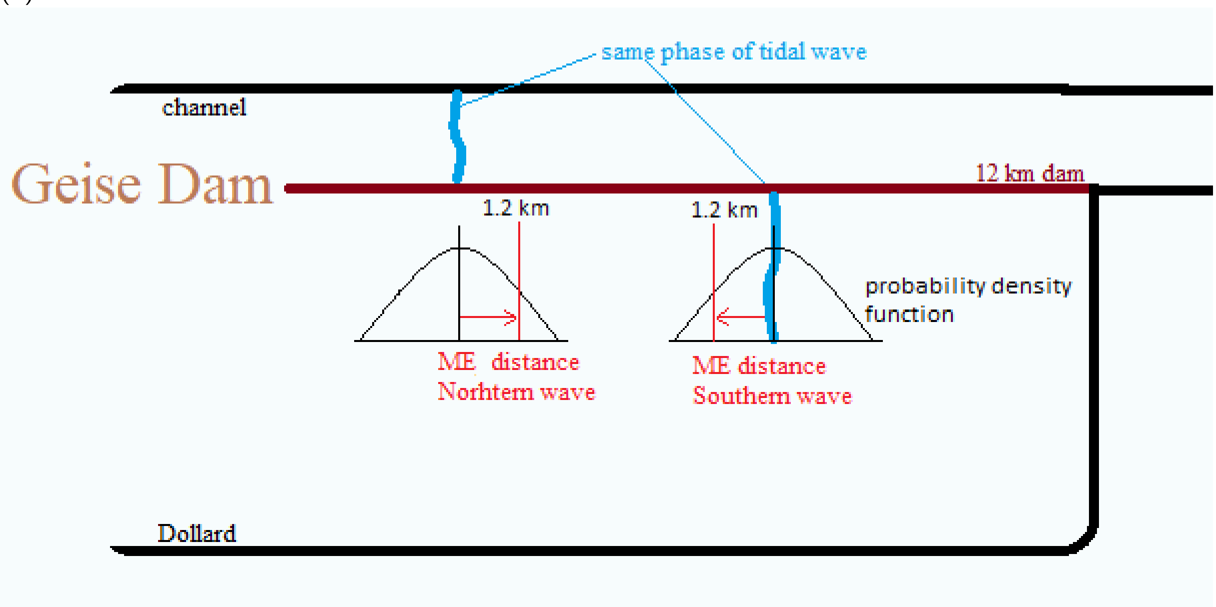

Figure 3.5: *Sketch of theory behind the interpretation of the velocity phase uncertainty. Figure (a) shows the ME of the rising tide, and (b) shows ME of the falling tide. The blue two blue waves represent the max ebb or flood phase of the tidal waves above and below the dam. These serve as a spatial reference point of the location of the tidal wave. The two black arches represent a unknown probability density curve with space on the x-axis and the probability on the y-axis. The two red lines give the Mean error (ME) distance of the reference point. As long as the Mean Errors of both waves do not overlap, the occurrence of a North-South water gradient flip seems unlikely.*

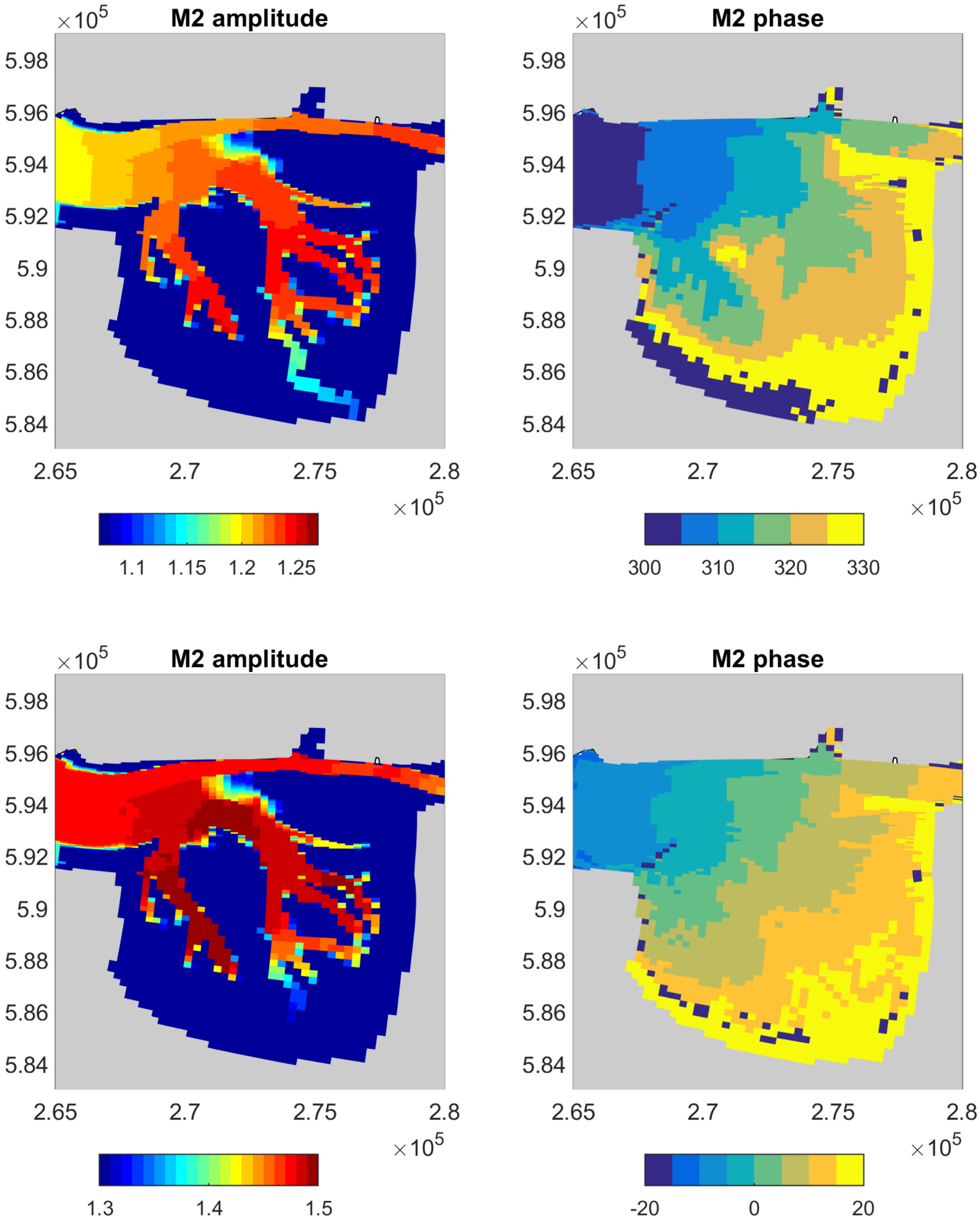

Figure 3.6: *This figure shows the propagation of the tide based on the reference modelling scenario with dam height 0.5. This resulting from the Fast Fourier Transform (section 2.3.6). The figures on the right show co-tidal lines linking locations of equal tidal phase. The figures on the left shows co-range lines linking the locations of equal tidal amplitude. The upper two graphs give the propagation during spring tide and the bottom graphs the propagation during neap tide.*

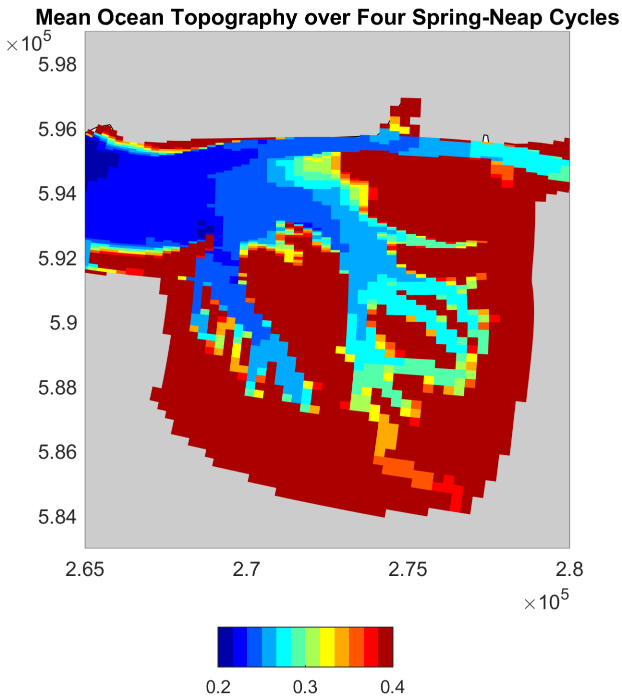

Figure 3.7: Mean ocean topography of 2019 over two spring neap tides based on a Fourier analysis.

to 30% more than in the Dollard. This can likely be contributed to the larger geometry of the Dollard, such as its the larger westerly entrance. The wider character of entrance bathymetry continues in the South-West direction, causing the tide to maily refract and slow down in that same direction.

Figure 3.7 shows the mean sea water levels over two spring-neap cycles. For the mean ocean water level, a similar gradient pattern is observed as in the phase plots. In the Fairway and the channels of the dollard a water level gradient is present in the along-chanel or streamwise direction. At the location of the dam there is a positive North-South water level gradient from the Fairway to the Dollard.

The combined insights from the average water level with the phase maps from Figure 3.6, suggests that the propagation of the M2 tide adapts cross-isobath behaviour as the gradients of the water level and phase mostly align. The alignment remains at the location of the dam and so suggesting a residual flow from the Dollard to the Fairway over the Geiseleit dam. Compared to the gradient of the phase, the positive North-South mean water level gradient is less clearly observable upstream of the harbour of Emden. This, because the averaging procedure was distorted by land that falls dry resulting in too higher values compared to the surrounding mapped area. Still, a positive North-South gradient can be observed when looking across the coordinate 2.77 in Figure 3.7. Here you see that the outer branches of the Dollard have a higher water level than the level in the Fairway present at the same longitude. Despite this, no concrete statements could be made on the water level gradient at the East side of the Geiseleit dam.

3.3 Tidal ellipses

Figure 3.8 shows tidal ellipses of the M2 tide near the dam obtained through the Fast Fourier transform described in Section 2.3.6. Similar to the analysis performed to obtain the amplitude and phase of the M2, this analysis was also based to two spring neap cycles. The ellipses describes the movement of the tip of the velocity vector of the M2 current. In the main channels of the Dollard and Fairway the tidal ellipses are almost flat and point in the stream-wise direction. This indicates that the tidal motion predominantly moves back and forth along the channel.

A circulation cell is visible such as the hypothesis by Van Maren et al. [2021] described in the introducion. The M2 ellipses refract towards the sandbank near the harbour of Emden (latitude $2.74{*}10^5$) towards the Geiseleit dam. This more shallow sandbank present along the entire Geiseleit dam. Viewing from the Dollard to the North, the tidal ellipses change direction in an anti-clockwise direction, and so does the propagation of the M2 current. At the same latitude ellipses show that the M2 current refracts in the clock-wise direction from the Fairway on to the sandbank. Another observed characteristic from the tidal ellipses is that the ellipses open up as they approach the dam its sandbank. With 'opening up' is meant that the velocity component along the semi-minor axis of the tidal ellipse increases relative to that of the semi-major axis. The Opening ellipses implies that the M2 tide propagates less back and forth and more elliptically on the sandbank compared to in the channel. Both dam-ward change in orientation of the ellipse and the opening of the tidal ellipse contribute to a cross-dam velocity component. This component closes the before aforementioned circulation cell over the Geiseleit dam.

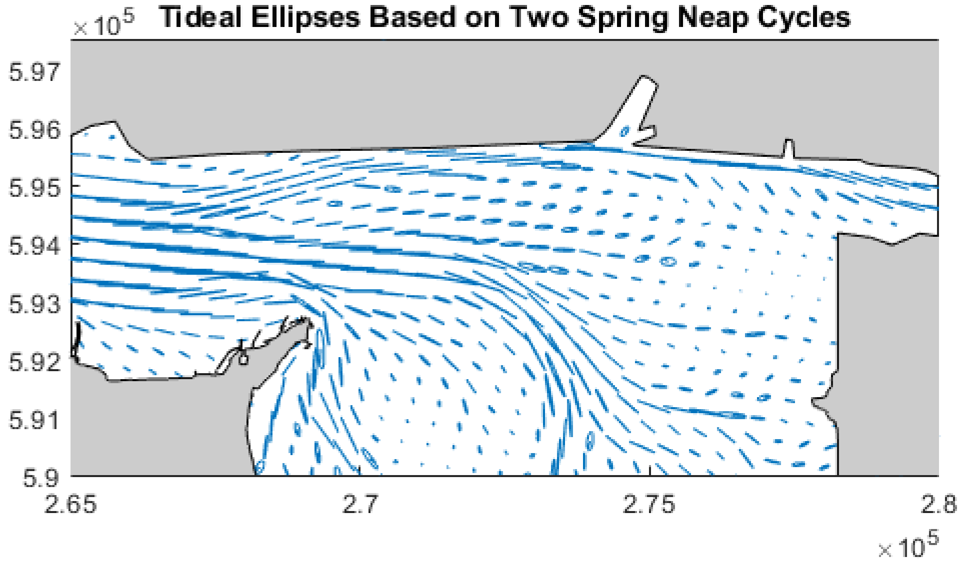

Figure 3.8: Tidal ellipses of the M2 tide based on a Fast Fourier Transform over the period of two spring-neam cycles. The figure illustrates how the tidal ellipses refract towards the dam its sandbank near the harbour of Emden, Confirming the exitance of the residual circulation cell as hypothesised by Van Maren et al. [2021]

3.4 Stokes transport and Eulerian and Lagrangian vector fields

Figure **??** displays a vector map containing Mean Eulerian, Stokes and Lagrangian velocity vectors. This figure shows the vector map of the reference scenario with a dam height of 0.5 meters. As more elaborately explained in Section 2.3.7, the Eulerian average is based on an average period spanning two spring-neap cycles, which equals 30.02 days or 58 periods of the M2 constituent. The Stokes drift is based on that very same period (see the limits of the definite integral in Equation 2.5 and 2.6). The Lagrangian can be seen as the net effect of the Mean Eulerian flow and Stokes drift as it is the sum of the two.

The Magnitude of the three vectors was observed to vary over space according to with the local depth. In shallower areas, such as on the sandbank near the Geiseleit dam, the Stokes drift was large in contrast with an smaller average Eulerian flow. In deeper areas such as the middle of the Fairway, the opposite was the case. Here, the average Eulerian velocities were mostly larger than the stokes transport. was The Stokes was observed to range from roughly 2 to 10 cm/s, which corresponds with the common order magnitudes of 5 cm/s such as as given in Uncles and Jordan [1979], Dronkers [2005] or 2 cm/s as presented in Dyke [1980]. Average Eulerian velocities ranged from 2 to a maximum of 20 cm/s . Net Lagrangian velocities ranged from 4 cm/s to a maximum of 40 cm/s at the West side of the Fairway.

The propagation of the Tidal wave results in stokes transport that is directed from the Dollard onto the sandbank of the Geiseleit dam. The mass transport towards the sandbank is partly compensated by a residual Eulerian current that is directed Westward along the Geiseleit Dam (see Figure 3.9, along latitude $5.945 * 10^5$ near the Harbour of Emden). This phenomena seems similar, but not the same, as the long-shore residual Eulerian current mentioned in [Tarya et al., 2010]. In contrast, results of this study show a mean Eulerian counter current on the sandbank of the Geiseleit dam that does not exactly opposes the Stokes Drift. Instead, the mean Eulerian counter current is more or less perpendicular to the Stokes drift. As a net effect of these two vectors, the Lagrangian mass transport still points in a northwest direction across the Geiseleit Dam. This suggests mass transport across the Geiseleit dam.

At the southern West-side of the dam near the entrance of the Lower Ems river, the Stokes drift has the same direction as the the Eulerian residual vectors. This results in a northward residual Lagrangian mass transport. However, the residual mass transport does not completely reach the dam as it the refracts West just South of the dam. Here, a in a deeper channel is located where the flow switches to a regime in which the mean Eulerian flow is compared the stokes drift smaller. Lagrangian flow over this part of the dam not completely oriented along the Geiseleit dam. This still results in a small northward residual flow over the dam.

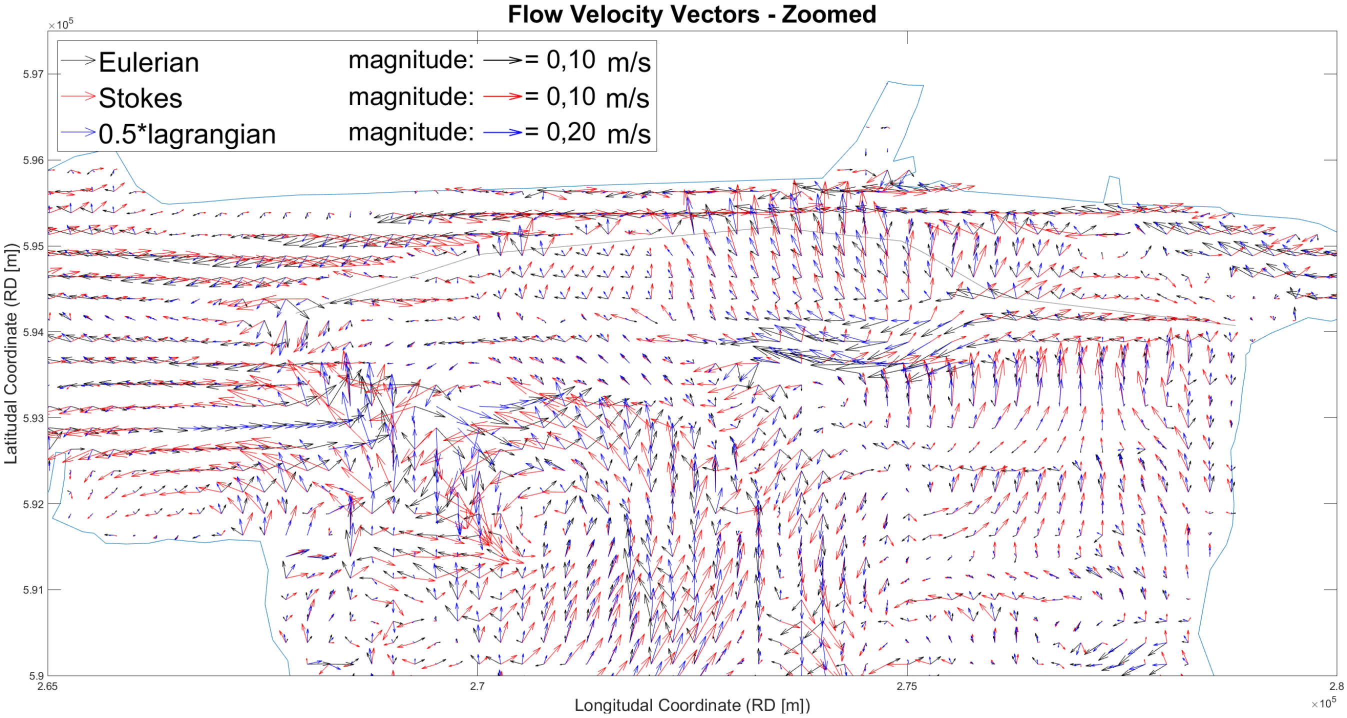

Figure 3.9: Mean Eulerian, Stokes and Lagrangian velocity vectors based on the reference scenario with a dam of 0.5m.

The figures provided in Annex A.3 display separate plots of the three different velocity vectors. This way, the velocity vectors can be viewed in more detail.

3.5 Effect of the Geiseleit Dam on local hydrodynamics

3.5.1 Cross-dam cumulative discharge

Table 3.1 presents the accumulative discharge calculated across the the Geiseleit dam for three dam height scenarios over a model period of 35 days. The sections: West, Mid and East, correspond to sections 1, 2 and 3 from Figure 2.2. Cumulative discharge for the impermeable dam scenario is per definition zero, so this scenario is only used in Figures 3.10 and 3.11 to illustrate the effect of the dam on the Stokes drift and the propagation of the tidal wave.

Table 3.1: Cumulative discharges across three dam sections, West Mid and East (see Figure 2.2).The table shows the cumulative discharges over a period of 35 days, from 24 to 28 January 2019.

	$Q_{cum}(m^3 \cdot 10^8)$			
Dam Height (m)	Entire Dam	West	Mid	East
0.0	+4.0	-3.5	+6.5	+1.0
0.5	+1.0	-4.5	+4.8	+0.7
1.0	-1.9	-4.7	+1.9	+0.9

* Q_{cum} is the accumulative discharge over a Dam section.
\+ indicates a northward flux and - a southward flux.

Due to the propagation of the tidal waves at the North and South side of the dam, a back and forth mass flux is induced across the dam. The accumulative discharges presented in Table 3.1 are a result of a surplus of flow over the dam. A typical characteristic of the surplus, or residual flow, is that it is created at the time scale of one tidal wave. This surplus was *not* created at the time scale of a spring-neap cycle. This, as only a marginal cumulative discharge increase was observed over the time scale of a spring-neap cycle. The cross-dam discharge surplus contributed by a spring-neap cycle was an order of magnitude smaller compared to the contribution observed at the time scale of a single tidal wave.

This table shows that a net northward flux is modelled for the Mid section and net southward flux for the West section. This fits with the hypothesis of circulation over the Geisedam proposed by Van Maren et al. [2015]. In addition, a smaller mass northward flux was observed from the Dollard to the Fairway over the East section. The residual flow across the East part of the Geiseleit also appears to contribute to the residual circulation over the Geiseleit dam. west and mid decrease heigher dam breaks circulation

The residual circulation pattern over the Geiseleit dam seems to reduce when the dam gets higher. Likely, the a higher dam adds more resistance to the flow across the dam, reducing the surplus of each tidal cycle. Section 3.5.3 elaborates on this. As the dam height increases, a decrease in cumulative discharge was modelled over the total of the Mid and East dam section. In contrast, an increase in accumulative discharge is observed for the west section.

The 0.5 m reference scenario shows the strongest circulation *over* the dam as the cumulative discharge over the northward and southward residual mass fluxes oppose each other the most. This in turn results in the lowest value for the total flux over the Entire dam.

The increasing dam height seems to stimulate the participation of a northward residual transport across the Mid section. The reason for this decrease can be found in the reduction of the northward transport of over the Mid and East dam section and the fact that the opposing residual flux over the west side of the dam stays roughly the same. The stimulated participation of the residual transport over the Mid section enhances the total northward residual flow from the Dollard into the Fairway.

According to the 0.0 and 0.5 meter scenario the total northward residual flow over the entire dam seems to decreases for an increasing dam height. Considering the 0.5 and 1.0 meter scenario, the residual flow seems to further decrease till it reverses to a southward flux, flowing from the Fair way to the Dollard.

3.5.2 Dam effect on Stokes, Eulerian and Lagrangian velocities

Velocity vectors of Stokes drift, the Eulerian mean and Lagrangian flow were plotted for different dam scenarios. These plots are presented in Figure 3.10. The figure shows three scenarios with different dam heights (plot a, b and c) and one scenario with an impermeable dam (plot d).

First we consider mass flow over the sandbank of the Geiseleit dam near the harbour of Emden. Here, an increase in magnitude of the mean Eulerian velocity vectors was observed for a decrease in dam height. At this location, the Stokes drift was also observed to increase for an decrease in dam height. Moreover the mean Eulerian starts to act less as a counter current to the Stokes drift. The previous subchapter elaborated on how the stokes drift perpendicular to the dam partly leads to mass compensation by a mean Eulerian current in the westward direction along the dam. When the dam gets lower, the orientation of the Eulerian current changes northward. As a result the Eulerian vectors and Stokes vectors align resulting in a larger northward Lagrangian mass transport. The above suggests that, the lower the dam the more northward mass transport over the Geiseleit dam near Emden. This is consistent with the observed Accumalative discharge across the mid-section of the dam from Table 3.1. The daily average northward cumulative discharge over the mid-section increases form $0.5 * 10^7$ to $1.9 * 10^7$ m^3 from a 1 meter dam scenario to a 0 meter scenario.

Secondly, we Consider the mass flow over the east side of the Geiseleit dam near the entrance to the Lower Ems river. In Section 3.4 we discussed how the net lagrangian flow turns west just south of the Eastern part of the dam, likely due to the presence of a deeper channel. The results of Figure 3.10 show that the residual flows in this channel alter according for different dam scenarios. The results show that the higher the dam, the more the residual Lagragian mass transport is directed through the channel westward along the Geiseleit dam. In the 0.0 meter dam scenario, the Lagrangian velocity vectors are oriented to the North-Nest, whereas these vector in the 0.5 and 1.0 meter dam scenario are oriented West. The North-West orientated vectors in the 0.0 meter scenario have a greater North component than that of the more westward pointing vectors in the 0.5 and 1.0 meter scenario. This suggests that the lower the dam, the higher the northward Lagrangian mass flux over the dam.

The suggestion above partly matches the calculations made for the accumulative discharge provided in Table 3.1. The northward accumulative discharge in the 0.0 meter scenario is indeed larger than that of other two other height scenarios. However, the accumulative discharge is higher for the 0.5 meter scenario than the 1.0 meter scenario. This is like the case because the 1.0 meter scenario has slightly larger, and more Northerly oriented Lagrangian vectors at the Easterly tip of the Geiseleit Dam.

The difference between between the accumulative discharge of different the height scenarios, is more similar over East side of the dam compared to over the the Mid and West section. This indicates that the impact of the dam height on the surrounding hydrodynamics is relatively less at East side of the dam. The hydrodynamics at East part of the dam are likely more determined by the sandbank as the sandbank is significantly larger compared to the bank at the mid and west section.

3.5.3 Dam effect on tidal wave propagation

Section 3.5 on the total cumulative discharge over the Geiseleit Dam, described that the residual flow over the dam mainly derives from a mass transport surplus happening at the time scale of a single tidal wave. This section closer inspects the influence of the dam on the propagation of a single tidal wave.

The Figures A.2, A.3, A.4 and A.1 in Annex A.1 show the propagation of a single tidal wave for the different dam scenarios. The propagation is illustrated by means of a multiple plots that show the water level at different stages of the propagation of the tidal wave through the study area. The different stages show the water level at: Max Rising Tide, 30 minutes before hight tide, high tide, max falling tide, 30 minutes before low tide and low tide. The timing of the tidal wave stages varies over space. For this reason the velocity time series of BM-GEI - a location just at the west side of the dam - was used as reference location to get the stages.

Along with each water level plot a map of the instantaneous Eulerian velocity vectors is provided to show get an image of what each stage means in terms of the flow velocity throughout the study area. Figure 3.11 shows an exemplary water level plot such as can be found for multiple stages and scenarios in Annex A.1.

The main outcome of the tidal propagation Figures shown in Annex A.1, is that a tidal wave at the that propagates through the Dollard propagates slower in upstream direction compared to the tidal wave in the Fairway. This characteristic can especially be well observed in the scenario with an impermeable dam. In this scenario the water level difference across the dam near Emden reaches a maximum of 18 cm. Throughout the falling tide, the water level difference is only marginal compared to that of the rising tide. More importantly, no cross-dam flow is possible as the Geiseleit dam is not submerged anymore.

A increase in dam height seems to enlarge the positive southward water level gradient during rising tide, suggesting less mass transport across the Geiseleit dam. From these figures can also be observed that a higher dam results in a longer time period in which there is a positive southward water level gradient. This can be seen back in the total cumulative discharge across the dam, discussed in section 3.5.

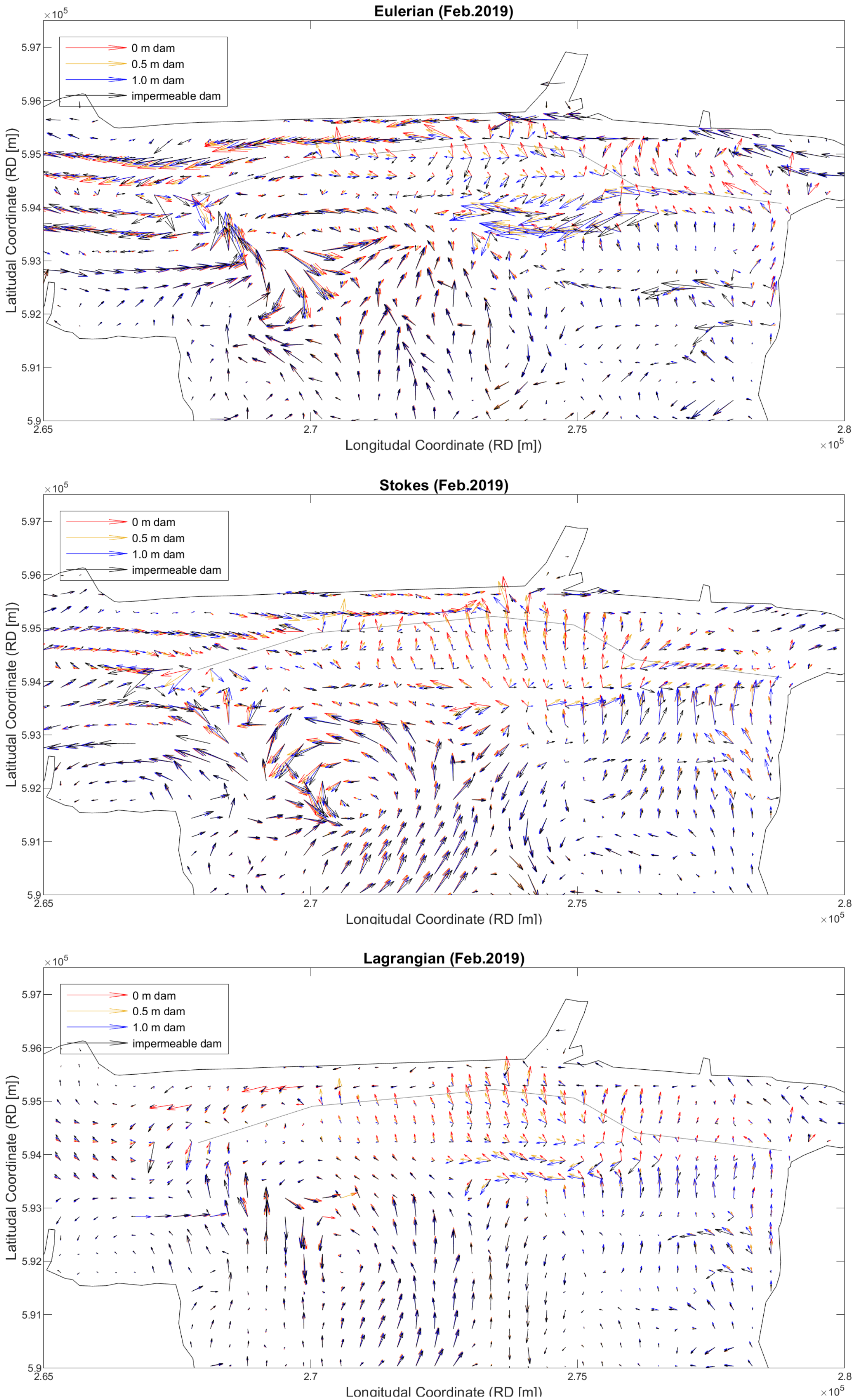

Figure 3.10: *This figure illustrates the time averaged Eulerian (a), Stokes (b), and Lagrangian (c) residual velocity vectors.The aggregation period used to calculated Stokes drift and the mean Eulerian velocity vectors is 30.02 days (two spring neap cycles).*

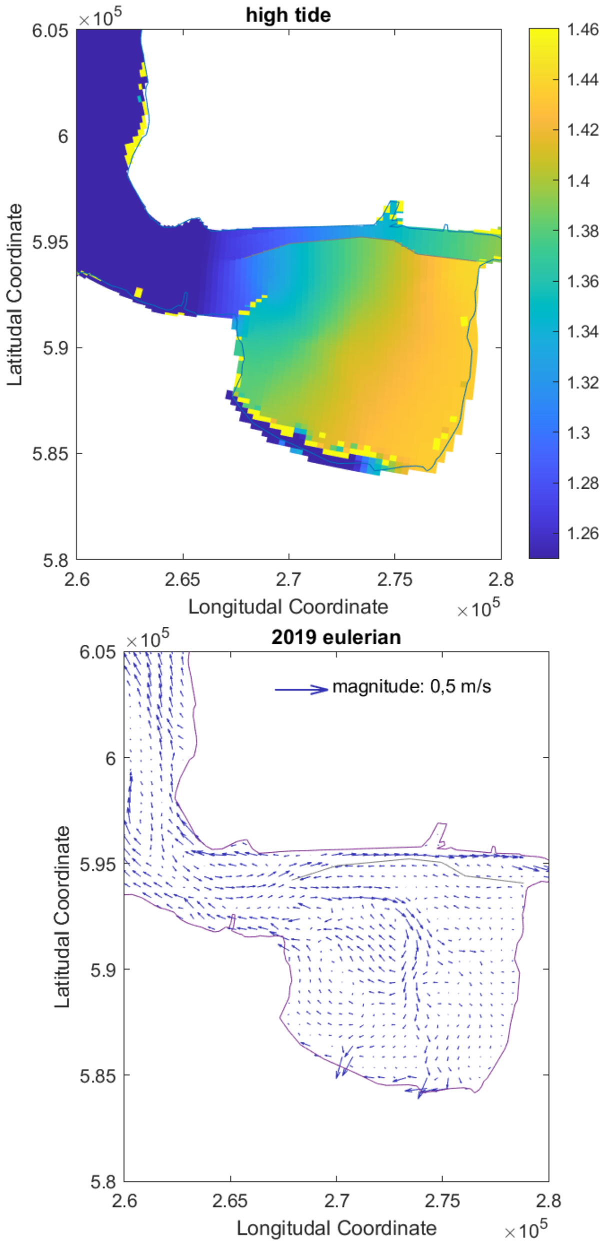

Figure 3.11: Caption example impermeable dam ocean-topo and eulerian mean 30.02 days

4 | Discussion

4.1 On the hypothesis of Residual circulation over the Geiseleit Dam

I found that there is a residual Stokes Drift of about 7 cm/s points across the dam and over the sandbank of the Geisesteert. This results in a residual Lagrangian mass transport from the Dollard in to the Fairway of Emden, crossing the Geiseleit dam at Emden. The northward mass transport supports the hypothesis of Van Maren et al. [2021] which states that a horizontal circulation cell is present. Van Maren et al. [2021] hypothesises that this cell is composed of residual flows that flow from the Dollard into the Fairway near Emden, and back via the Ems estuary into the Dollard.

In contrast to my findings and the hyphothesis of Van Maren et al. [2021], older studies such as Pein et al. [2014] had not reported on the existence of this residual circulation cell. Pein et al. [2014] studies residual circulation patterns in the Ems Estuary and presents five residual barotropic circulation cells downstream of the Geiseleit dam. However this study does not recognise a residual cell over the Geiseleit dam despite the fact that the tidal flat of the Geiseleit dam was included in their Analysis. Likely the cell was not observed as only residual Eulerian velocities were modelled, not any stokes drift. Another reason could be the course grid resolution of this modelling study.

4.1.1 Residual Stokes drift, a missing link?

My results suggest that Stokes Drift is the dominant hydrodynamic mechanism that drives the residual water mass transport over the Geiseleit Dam near Emden. This Stokes drift is based on the wave action of the tidal wave that propagates onto the Geisesteert south of the dam near Emden. My analysis of the tidal propagation and cumulative discharge over the Geiseleit dam confirms that the driving hydrodynamics behind this sediment transport happens at the time scale of ebb-flood cycles.

Based on the results of this study, follow up research can further develop the used Delft3D-FM model to get insight in the interaction between the Hydrodynamics, such as the Stokes drift over the dam, and residual sediment fluxes over the dam. Follow up research can use the Lagrangian velocities produced by the model and data analysis to further asses hypotheses made on sediment transport across the Geise dam.

Two hypothesis on the sediment dynamics were made by Dyer et al. [2000] and Van Maren et al. [2021]. Dyer et al. [2000] argues that a net northward sediment transport over the Mid dam section is driven by a combined process of sediment settling and re-suspension that is induced by wave action. The obtained insights on the residual flow velocities of this modelling study should be combined with insights on the mechanism of (re-)suspension to provide insight in sediment dynamics of the study. Moreover, Van Maren et al. [2021] hypothesises how storm conditions can enhance the re-suspension of sediment due to more energetic wave action. Sediment is first deposited onto the Geisesteert, a sandbank south of the Geiseleit dam, and than further transported to the Fairway. Despite this, Van Maren et al. [2021] did not determine the temporal episodic character of the residual sediment. Further attempts can be made to study this episodic character now that we know that Stokes transport is the missing hydrodynamic link explaining the presence of a circulation cell. More specifically, more research to identify the mechanisms behind residual sediment fluxes. This through linking to sediment advection by tidally driven Stokes drift, to the temporally varying wave suspension processes based on wind induced wave action.

4.1.2 Residual flow over the West dam section

In contrast to this hypothesis, my findings suggest a residual circulation pattern which, not only involves southward flows at this junction, but also involves a southward residual transport over the west side of the dam. This difference is likely explained by the fact that the modelled bathemetry is too coarse to include the elevated sandbank present around the Geiseleit dam at the Westerly tip of the Geiseleit dam. At this location the Geiseleit dam reaches a height of 1 meter above NAP according to Van Maren et al. [2021]. However, in the bathymetry of my model, the height of the sandbank on which the Geiseleit dam is placed turns out to be 1.6 meter below NAP (see Figure 4.2). So even when a Geiseleit dam of 1 meter was implemented on top of the model bathymetry, the modelled dam would still be

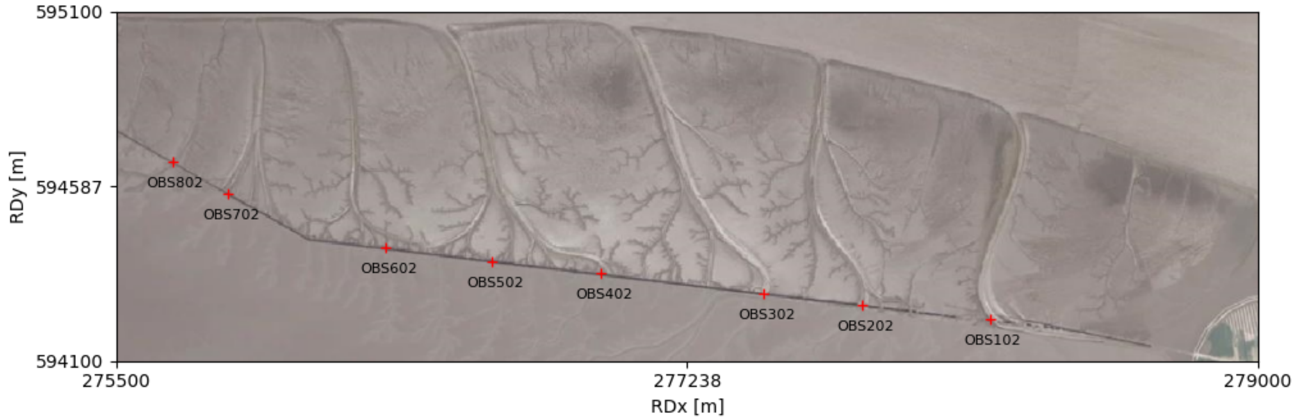

Figure 4.1: *ADCP measurements locations at the East side of the Geiseleit dam from the EDoM measurement campaign of January-February 2021 Van Maren et al. [2021]. This Satellite image shows the drainage channels that were smoothed in the model bathemetry.*

submerged by about 0.5 meters. This could explain why the western side of the circulation cell over the dam was located more to the East instead of at junction of the Dollard and the Fairway.

The effect of the low bathymetry was not noted in the model validation as the model produced velocities that matched the ADCP measurments well. This indicates that this effect only marginally affected the flow in the main channels where the ADCP measurment points were located. Hsu et al. [1999] stresses the importance of considering the extent to which a validated point is valid over space. The certainty of a locally verified point at which observed and model data is compared, can decrease quickly over space. This, as current velocities could vary rapidly form point to point in space depending on the Bathymetry. For this reason modelling of residual flow over the Geiseleit dam should include the recently added calibration points on the Geiseleit dam.

Still the model seem usefull for capturing the main hydrodynamics of the Dollard and the Fairway such as the propagation of the tidal wave. This, because the model configuration is similar to the model configuration based on water level calibration performed by Schrijvershof et al. [2022]. According to Hsu et al. [1999] the calibration of estuaries models using water levels includes less spatial uncertainty.

No further model adjustments were made besides those from Table 2.1. This considering that it would be realistically hard to obtain further improvement of the model with regard to the ntr as it is only set up to model (2D) barotropic hydrodynamic mechanisms. Non tidal residual flow processes can also be linked to baroclinic mechanisms, such as estuaries circulation. [Dronkers, 2005]. Adjusting the model for baroclinic mechanisms is useful, but beyond the scope of this research. For further research, model improvement can be made by calibrating with ADCP observations done on the Dam, recently presented in Van Maren et al. [2021].

4.1.3 Residual flow over the East Dam section

Furthermore, the residual mass transport modelled at the East side of the dam was mainly directed in the along-dam direction which resulted a small northward Lagrangian mass transport. This result seems in disagreement as this opposes the direction of recent ADCP observations made during march 2021 Van Maren et al. [2021]. The flow direction observed measurement points OBS702 and OBS802 from Van Maren et al. [2021], located between first and second bend, show a less evident southward residual flux. Despite this it still does not locally match the model results.

This disagreement can partly be explained by how the East dam section is defined in this study. The East section reaches to the second bend looking from east to west (see Figure 2.2). Between the first and second bend, a relatively large northward Lagrangian flow was modelled. This has resulted in a summed northward transport over the entire East section of the dam.

Similar to the fluxes over the West side of the dam, the disagreement may also be due to fact that the modelled bathymetry was too coarse to include the drainage channels that can be seen in Figure 4.1. These channels are more then 2 meters deeper than the surrounding sandbank, even at some places at the Geiseleit dam.Van Maren et al. [2021] The model critically fails to model the residual flow through the deeper channels illustrated in Figure 4.1. The Dollard and Fairway are therefore better connected than how it was modelled.

The disagreement puts the importance of these channels in perspective. Without the existence of these channels, flow would mainly occurs in the direction along the dam. Based on my model results and the observation of Van Maren et al. [2021], the channels at the error shows that the channels I could also have been the implementation of the dam height.

As a last note on the residual flows at the East-dam section, A residual up-estuary transport was observed along the southern bank of the Fairway (see Figure 3.9). The existence of this residual flow was also mentioned by Van Maren et al. [2021]. This residual flux is used to hypothesise about how lateral and vertical salinity driven estuarine circulation results in up-estuary sediment transport (see Figure 3-23 of Van Maren et al. [2021]). In contrast with this hypotheses the modelled barotropic residual flow of in this theses does not reach all the way up to the entrance of the lower river. More research is needed on the interaction between river flow dynamics and the up-estuary residual flow at the entrance of the lower Ems river.

4.2 Hydrodynamic Mechanisms

4.2.1 Mechanisms moderating residual circulation over the Geiseleit dam

The main outcome of the results of this thesis is confirmation of the existence of a residual circulation cell over the Geiseleit Dam as result of a difference in propagation of the tidal wave north and south of the dam. The residual circulation cell over the dam is driven by on-bank Stokes transport. Literature suggests that different processes determine the persistence of residual circualtion in the Ems estuary.

The study of De Jonge [1992] agrees with the existance of residual mass circulation over the Geiseleit Dam. In contrast to Van Maren et al. [2021] this study hypothesises about the presence of a northward residual flux over, what I called the East dam section. The persistence of this residual circulation cell was said to be moderated by depth average drift currents on shallow part of the Dollard, matching the observation that the residual transport happens through Stokes drift over the shallows of the Geiseleit dam.

Another moderater for the residual circulation is the (varying) river discharge travelling though the Fairway. This, as the tidal water transport was observed to be of similar magnitude compared to the river discharge.

4.3 Geiseleit Dam effect on Hydrodynamic Mechanisms

4.3.1 Dronker's Model of Equilibrium Length

Chapter 6 of Dronkers presents a model for the convergence length of an estuary. The convergence length describes the estuarine geometry for which an estuary is the morphologically stable. The model explains the commonly found funnel shape of estuaries by relating the width of the estuary to the total shear stress and sediment sediment transport. If the convergence length is longer than the equilibrium convergence length, the estuary is too wide tidal inflow looses less energy due to shear, leading more inward sediment transport and infilling of the estuary. This infilling in turn leads to an increase in shear leading to less sediment import, bringing the estuarine geometry back into equilibrium.

From down to upstream, Dronkers defines three zones in which different hydrodynamic mechanisms drive sediment transport. Most upstream the influence of tide is little compared to that of the river. More downstream the sediment transport is driven by a mix of river and tidal component. Even more downstream the influence of the river on the sediment transport becomes very small compared to that of the tide. The relation between the hydrodynamic mechanisms and sediment transport for the these three zones is presented with formulas 6.68 and 6.9. These formulas describe the sediment flux as based on the participation of Stoke Drift, river discharge and tidal asymmetry.

Considering this model for the equillibrium convergence length, one could argue that the Geiseleit dam affects the width and therefor the hydrodynamics of around the dam. As the Geiseleit dam affects the local width of the estuary, it shifts the location of these three zones described above. This shift alters degree of participation of the hydrodynamic mechanisms such as the influence of the river or that of the tidal asymmetry. The Geiseleit Dam makes up the Fairway with a relative small width compared to what would be expected from continuation of the funnel shaped estuary down stream. This relatively narrow width enhances the influence of

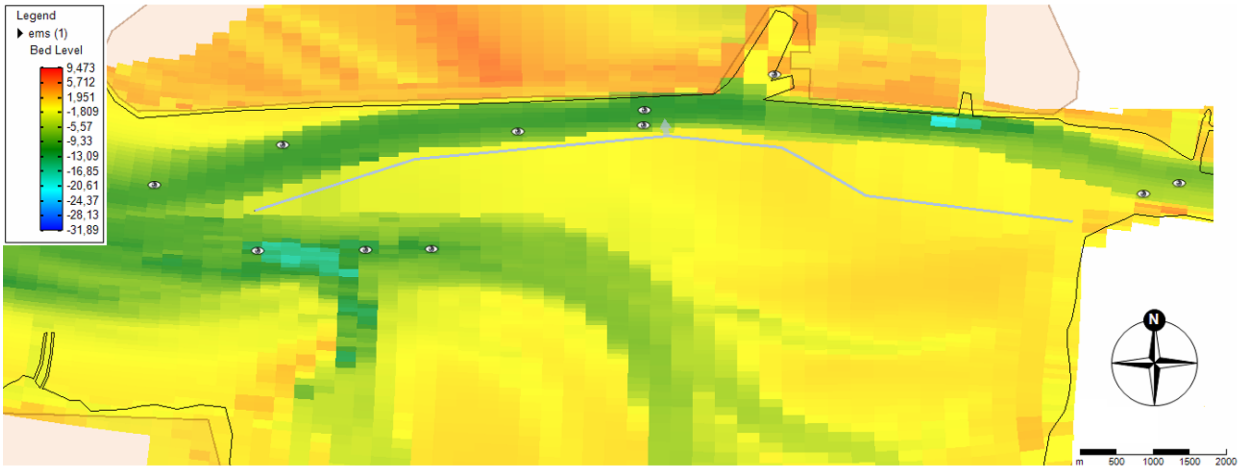

Figure 4.2: Model bathymetry at the Geiseleit dam

the river in downstream direction resulting in more sediment flushing by the river.

During flood, the total width of the Dollard and Fairway is much larger than what would be expected from the continuation of the funnel shape. If the Geiseleit dam would not exist, this width would suggests infilling. The Geiseleit dam makes sure that the river component in formula 6.69 of Dronkers [2005] stay high enough to prevent infilling and maintain a navigable depth of the Fairway.

My results show that the dam also induces a water level gradient, suggesting enhancement circulation over the Geiseleit dam, likely resulting more sediment transport from the Fairway into the Dollard.

Making the dam higher therefore does not per se mean that less dredging would be needed to maintain the Fairway depth. My results show that, at the one hand a higher dam could lead to less discharge across the dam. According to Dronkers [2005] this increases river flushing. On the other hand, my results show also that more flow resistant dam leads to a larger difference in tidal propagation and a larger water level gradient. More research is needed to asses how these two mechanisms balance eachoter. This in order to further determine the persistence of the residual circulation cell and its implications for sediment transport from the Dollard into the Fairway.

4.3.2 Residual transport with regard to tidal asymmetry

Pein et al. [2014] gives a detailed overview of flood- and ebb-dominant locations in the estuary. The tidal channel of the Dollard is ebb dominant. The Fairway is ebb-dominant till just west of the harbour of Emden, where it continues to be flood-dominant in the upstream direction. Even though the the flood dominance in the west side of the Fairway, the results of this thesis still suggest a ebb-directed residual current.

This contrasts with the idea of Pein et al. [2014] that the residual flows match with spatial patterns of flood and ebb dominance.

5 | Conclusion

Research question 1:

The model is well capable of reproducing the current measurements gathered at the interface of the Ems Easturary. The Edom ADCP meassurments matched the produced stream wise currents with a Skill Score of 0.99, and a RMSE of 0.15 m/s comparing to velocity amplitudes of about 1.5 m/s. in the stream wise direction. Currents in the stream-cross direction were modelled less well with a Skill Score of 0.53 and a RMSE of 0.027 m/s comparing to velocity amplitudes of about 0.035 m/s. Despite, less well modelled stream cross flow, conclusions could still be made on the hydrodynamics as the as the stream wise component was marginal compared to the stream wise velocity component.

The propagation of the tidal wave was modelled well enough to predict the direction of the long-term water level gradient. Mean Error between the observed and modelled phase at the max rising tide was 10 minutes and 25 minutes for that of max falling tide. Meaning the tidal waves should respectively be at least 0.9 km and 2.3 km apart in order not to flip the water level gradient.

Research question 2:

This study confirmes the presence of a residual circulation flow over the Geiseleit dam as hypothesised by Van Maren et al. [2021]. The main tide-induced mechanism that drives the residual circulation cell near Emden is a cross-dam residual Stokes' drift over the Geisesteert shoal. In perspective of the discussed literature [De Jonge, 1992, Pein et al., 2014], Stokes' drift is the missing driving mechanism that can explain the completion of a residual circulation cell over the Geiseleit dam.

This study revealed that a relative difference in tidal wave propagation celerity between the channel north and south of the Geiseleit Dam results in a cross-dam phase difference of the M_2 tide. The result is a northward refraction of the tidal wave onto the Geisesteert sandbank near Emden. The propagation over the Geisesteert leads to a Stokes Drift of 0.7 cm/s perpendicular to the dam, and a smaller residual Eulerian counter current Westward along the dam. The larger, more dominant Stokes' drift results in a net residual Lagrangian mass transport over the dam.

The inclusion of a smoothed model bathymetry and its resulting disagreement in residual discharge across the East part of the dam, stresses the importance of flow through Tidal Creeks. Modelling with a finer bathymetric grid is needed to better understand what these creeks mean for the residual flow patterns in the estuary.

Research question 3:

The effect of the Geiseleit Dam on the residual circulation over the dam is that, the higher the dam, the larger the long-term positive southward water level gradient. This gradient results in a greater Lagrangian transport over the dam near Emden, enhancing the residual circulation in the circulation cell.

A higher dam also lengthens the time that a positive southward gradient water level is present, especially during the start of the falling tide. This also leads to more cross- dam mass transport over the period of a tidal cycle. Cross-dam flow can be prevented by making the dam impermeable, and at least high enough not to be submerged by the passing tidal wave.

Acknowledgements

First and most of all, I want to thank my supervisors Ton Hoitink and Reinier Schrijvershof for their dedicated help throughout the entire process. I want to especially thank them for all the time and effort they took to provide me with extensive feedback. Moreover, I would like to thank Reinier for the weekly meetings we had. I appreciated the positive reinforcement that always pushed me to work to the best of my abilities. Really good guidance, well done!

Furthermore I would like to thank Deltaris, and the parties involved in the EDoM campaign to provide me with the data I used for my model calibration and validation. Last but not least, I want to thank my parents for their mental support, I could not have done it without them.

Bibliography

Marius Becker. Edom Mooring Chain TRBM ADCP processing, December 2018.

Franciscus Colijn, Wim Admiraal, Job W. Baretta, and Piet Ruardij. Primary production in a turbid estuary, the Ems-Dollard: field and model studies. *Continental Shelf Research*, 7(11):1405–1409, 1987. ISSN 0278-4343. doi: https://doi.org/10.1016/0278-4343(87)90045-8. URL https://www.sciencedirect.com/science/article/pii/0278434387900458.

Tanya J Compton, Sander Holthuijsen, Maarten Mulder, Maarten van Arkel, Loran Kleine Schaars, Anita Koolhaas, Anne Dekinga, Job ten Horn, Pieternella C Luttikhuizen, Jaap van der Meer, et al. Shifting baselines in the ems dollard estuary: A comparison across three decades reveals changing benthic communities. *Journal of Sea Research*, 127:119–132, 2017.

VN De Jonge. Tidal flow and residual flow in the ems estuary. *Estuarine, Coastal and Shelf Science*, 34(1):1–22, 1992.

Job Dronkers. *Dynamics of coastal systems*, volume 25. World Scientific, 2005.

KR Dyer, MC Christie, N Feates, MJ Fennessy, M Pejrup, and W Van der Lee. An investigation into processes influencing the morphodynamics of an intertidal mudflat, the dollard estuary, the netherlands: I. hydrodynamics and suspended sediment. *Estuarine, Coastal and Shelf Science*, 50(5):607–625, 2000.

PPG Dyke. On the stokes' drift induced by tidal motions in a wide estuary. *Estuarine and Coastal Marine Science*, 11(1):17–25, 1980.

Mary C. Hill. Methods and Guidelines for Effective Model Calibration. In *Building Partnerships*, pages 1–10, Minneapolis, Minnesota, United States, September 2000. American Society of Civil Engineers. ISBN 978-0-7844-0517-8. doi: 10.1061/40517(2000)18. URL http://ascelibrary.org/doi/10.1061/40517%282000%2918.

Ming-Hsi Hsu, Albert Y Kuo, Jan-Tai Kuo, and Wen-Cheng Liu. Procedure to calibrate and verify numerical models of estuarine hydrodynamics. *Journal of hydraulic engineering*, 125(2):166–182, 1999.

Royal Netherlands Meteorological Institute. Wind - Groups - KNMI Data Platform. URL https://dataplatform.knmi.nl/group/wind.

Lei Ji and Kevin Gallo. An Agreement Coefficient for Image Comparison. *Photogrammetric Engineering & Remote Sensing*, 72(7):823–833, July 2006. ISSN 00991112. doi: 10.14358/PERS.72.7.823. URL http://openurl.ingenta.com/content/xref?genre=article&issn=0099-1112&volume=72&issue=7&spage=823.

Ming Li, Liejun Zhong, and William C. Boicourt. Simulations of Chesapeake Bay estuary: Sensitivity to turbulence mixing parameterizations and comparison with observations. *Journal of Geophysical Research: Oceans*, 110(C12), 2005. ISSN 2156-2202. doi: 10.1029/2004JC002585. URL https://onlinelibrary.wiley.com/doi/abs/10.1029/2004JC002585. _eprint: https://onlinelibrary.wiley.com/doi/pdf/10.1029/2004JC002585.

M. S. Longuet-Higgins and R. W. Stewart. Radiation stress and mass transport in gravity waves, with application to 'surf beats'. *Journal of Fluid Mechanics*, 13(4):481–504, August 1962. ISSN 1469-7645, 0022-1120. doi: 10.1017/S0022112062000877. URL https://www.cambridge.org/core/journals/journal-of-fluid-mechanics/article/abs/radiation-stress-and-mass-transport-in-gravity-waves-CEE23C7B7F6776AA78150426A67B98BB. Publisher: Cambridge University Press.

D. S. van Maren, J. Vroom, and D. van Keulen. *Exchange processes between Ems river and estuary - DRAFT. Technical report*. 2021.

Jan-Willem Mol. ED2050 August 2018 metadata frame 1, September 2018.

Rich Pawlowicz, Bob Beardsley, and Steve Lentz. Classical tidal harmonic analysis including error estimates in matlab using t_tide. *Computers & Geosciences*, 28(8):929–937, 2002.

Johannes Ulrich Pein, Emil Vassilev Stanev, and Yinglong Joseph Zhang. The tidal asymmetries and residual flows in ems estuary. *Ocean Dynamics*, 64(12):1719–1741, 2014.

DT Pugh and JM Vassie. Extreme sea levels from tide and surge probability. In *Coastal Engineering 1978*, pages 911–930. 1978.

Praveen Rathod and Vivek L. Manekar. Comprehensive approach for scour modelling using artificial intelligence. *Marine Georesources & Geotechnology*, 0(0):1–15, February 2022. ISSN 1064-119X. doi: 10.1080/1064119X.2022.2035025. URL https://doi.org/10.1080/1064119X.2022.2035025. Publisher: Taylor & Francis _eprint: https://doi.org/10.1080/1064119X.2022.2035025.

Reinier Schrijvershof, D.S. Van Maren, and A.J.F. Hoitink. A synthetic representative tidal signal for long-term morphological modelling - Netherlands Centre for Coastal Research, February 2022. URL https://www.nck-web.org/boa-2022/485-a-synthetic-representative-tidal-signal-for-long-term-morphological-modelling.

Stefan Talke, Victor de Jonge, and Huib de Swart. Dynamics of estuarine turbidity maxima (etm): coupling of morphology and biology. https://webspace.science.uu.nl/~swart104/Ems_website/Ems_ETM_research.htm, January 2007.

Stefan A Talke and Huib E De Swart. Hydrodynamics and morphology in the ems/dollard estuary: review of models, measurements, scientific literature and the effects of changing conditions. 2006.

A. Tarya, A. J. F. Hoitink, and M. Van der Vegt. Tidal and subtidal flow patterns on a tropical continental shelf semi-insulated by coral reefs. *Journal of Geophysical Research*, 115(C9):C09029, September 2010. ISSN 0148-0227. doi: 10.1029/2010JC006168. URL http://doi.wiley.com/10.1029/2010JC006168.

RJ Uncles and MB Jordan. Residual fluxes of water and salt at two stations in the severn estuary. *Estuarine and Coastal Marine Science*, 9(3):287–302, 1979.

T. S. van den Bremer and Ø. Breivik. Stokes drift. *Philosophical Transactions of the Royal Society A: Mathematical, Physical and Engineering Sciences*, 376(2111):20170104, January 2018. doi: 10.1098/rsta.2017.0104. URL https://royalsocietypublishing.org/doi/10.1098/rsta.2017.0104. Publisher: Royal Society.

Karianne M van der Werf. A multidisciplinary perspective on the natural quality and rights of river systems: Would granting legal rights to the ems-dollard estuary in northwest europe benefit the natural system? Master's thesis, 2019.

Dirk S van Maren, Johan C Winterwerp, and Julia Vroom. Fine sediment transport into the hyper-turbid lower ems river: the role of channel deepening and sediment-induced drag reduction. *Ocean Dynamics*, 65(4):589–605, 2015.

Dirk S. Van Maren, Johan C. Winterwerp, and Julia Vroom. Fine sediment transport into the hyper-turbid lower Ems River: the role of channel deepening and sediment-induced drag reduction. *Ocean Dynamics*, 65(4):589–605, April 2015. ISSN 1616-7341, 1616-7228. doi: 10.1007/s10236-015-0821-2. URL http://link.springer.com/10.1007/s10236-015-0821-2.

Dirk Sebastiaan Van Maren, Julia Vroom, and Daan van Keulen. Exchange processes between the Ems river and estuary. Results of EDoM measurement campaigns 2018 2019. Technical report, Deltares, Delft, 2021.

Qiushun Wang and Cunhong Pan. Three-dimensional modelling of sediment transport under tidal bores in the Qiantang estuary, China. *Journal of Hydraulic Research*, 56(5):662–672, September 2018. ISSN 0022-1686. doi: 10.1080/00221686.2017.1397781. URL https://doi.org/10.1080/00221686.2017.1397781. Publisher: Taylor & Francis _eprint: https://doi.org/10.1080/00221686.2017.1397781.

John C. Warner, W. Rockwell Geyer, and James A. Lerczak. Numerical modeling of an estuary: A comprehensive skill assessment. *Journal of Geophysical Research: Oceans*, 110(C5), 2005. ISSN 2156-2202. doi: 10.1029/2004JC002691. URL https://onlinelibrary.wiley.com/doi/abs/10.1029/2004JC002691. _eprint: https://onlinelibrary.wiley.com/doi/pdf/10.1029/2004JC002691.

Hao Wei, Dagmar Hainbucher, Thomas Pohlmann, Shizuo Feng, and Juergen Suendermann. Tidal-induced lagrangian and eulerian mean circulation in the bohai sea. *Journal of Marine Systems*, 44(3-4):141–151, 2004.

Cort J. Willmott. On the Validation of Models. *Physical Geography*, 2(2):184–194, July 1981. ISSN 0272-3646. doi: 10.1080/02723646.1981.10642213.

URL https://doi.org/10.1080/02723646.1981.10642213. Publisher: Taylor & Francis _eprint: https://doi.org/10.1080/02723646.1981.10642213.

Anna Wunsche. Short report on processing of mooring chain data EDoM 2018, November 2019.

Appendix

A | Appendix

A.1 Tidal wave propagation per various dam scenario

This Appendix contains water level plots illustrating the tidal Wave propagation for the scenarios: 0.0, 0.5, 1.0 meter dam, and the scenario of a impermeable dam.

A.2 Target plots containing all measurement locations

This appendix contains Target plots featuringn the model improvement at each measurement location. The main text contains target plots in which the score are averaged across all locations.

A.3 Separate velocity vector plots per dam scenario

This annex shows separated zoomed plots of the residual Eulerian velocity vectors, Stokes Drift, and residual Lagrangian velocity vectors.

Impermeable Dam

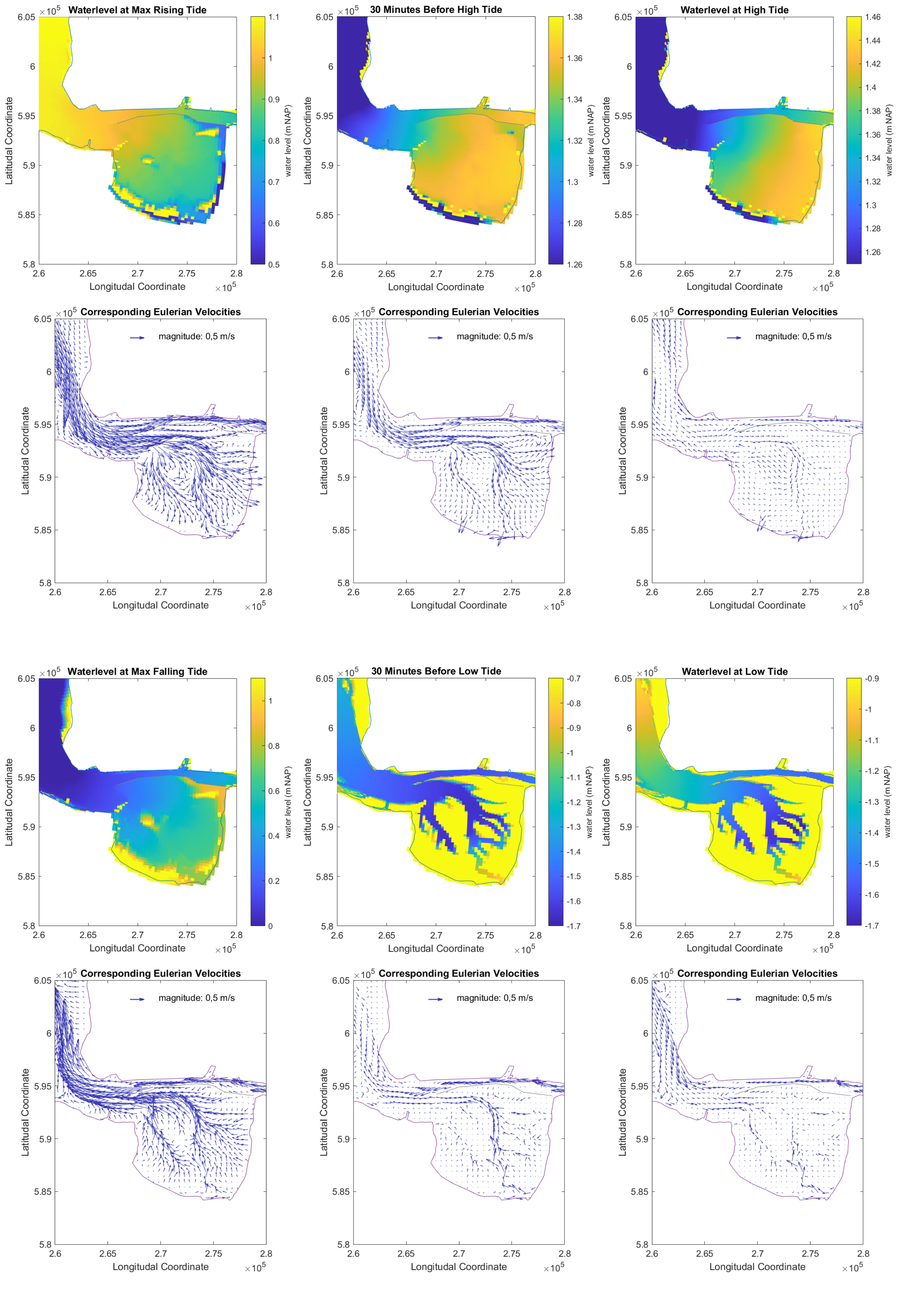

Figure A.1: *This figure shows the propagation of the tidal wave throughout an eb-flood cycle in the impermeable dam scenario.*

0.0 Meter Dam

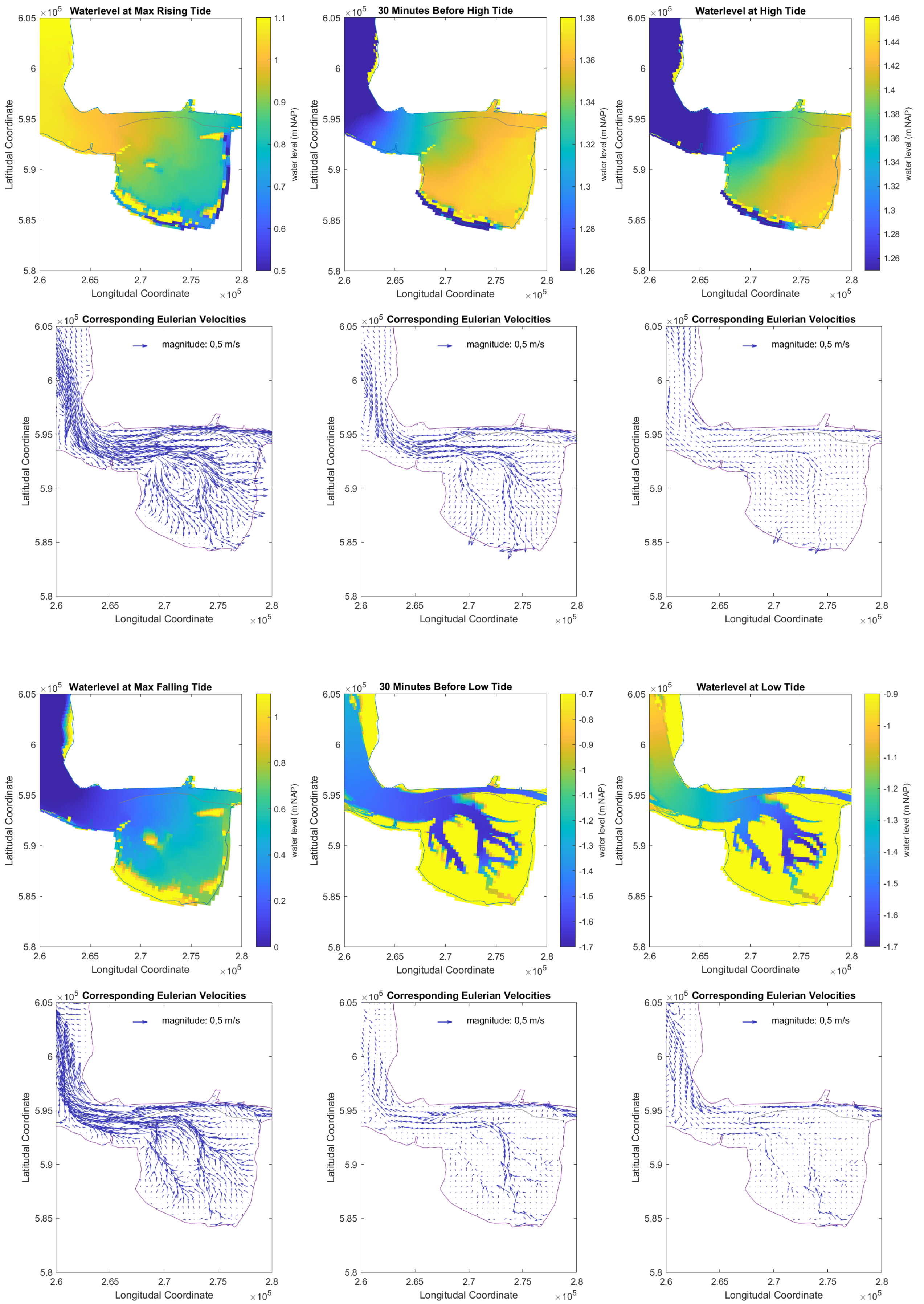

Figure A.2: *This figure shows the propagation of the tidal wave throughout an eb-flood cycle in a no dam modelling scenario.*

0.5 Meter Dam

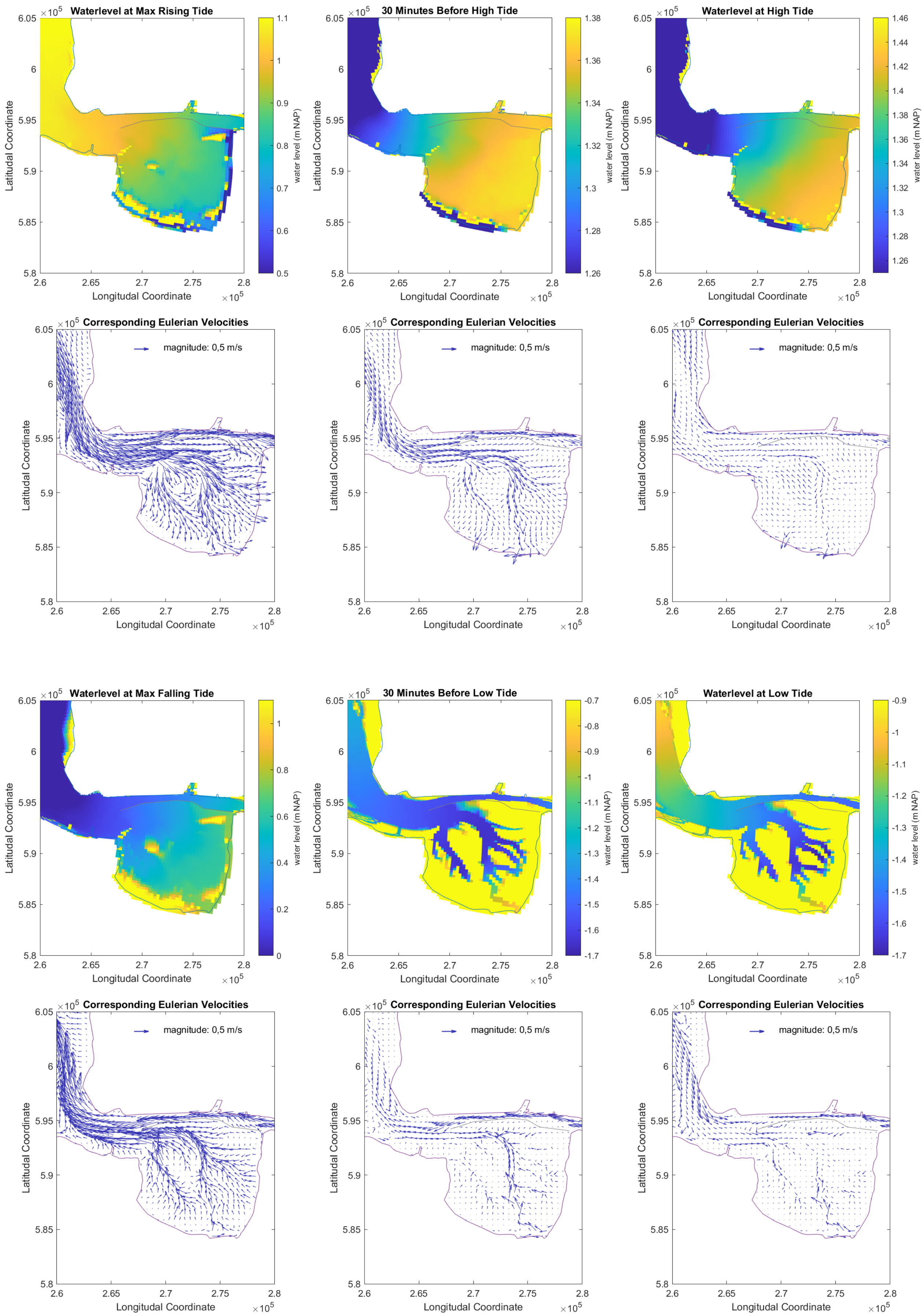

Figure A.3: *This figure shows the propagation of the tidal wave throughout an eb-flood cycle in a 0.5 meter scenario.*

1 Meter Dam

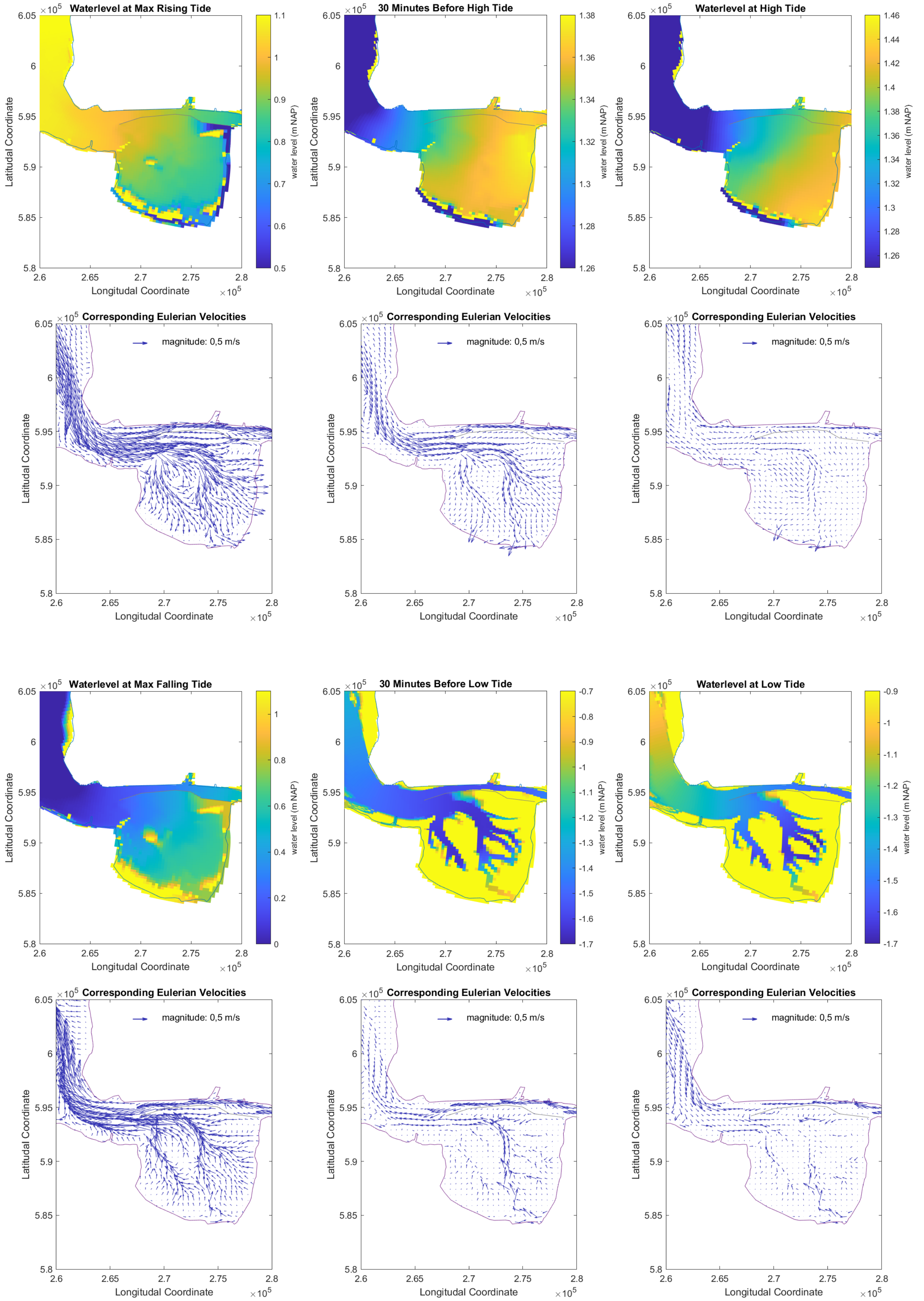

Figure A.4: *This figure shows the propagation of the tidal wave throughout an eb-flood cycle in a 1 meter scenario.*

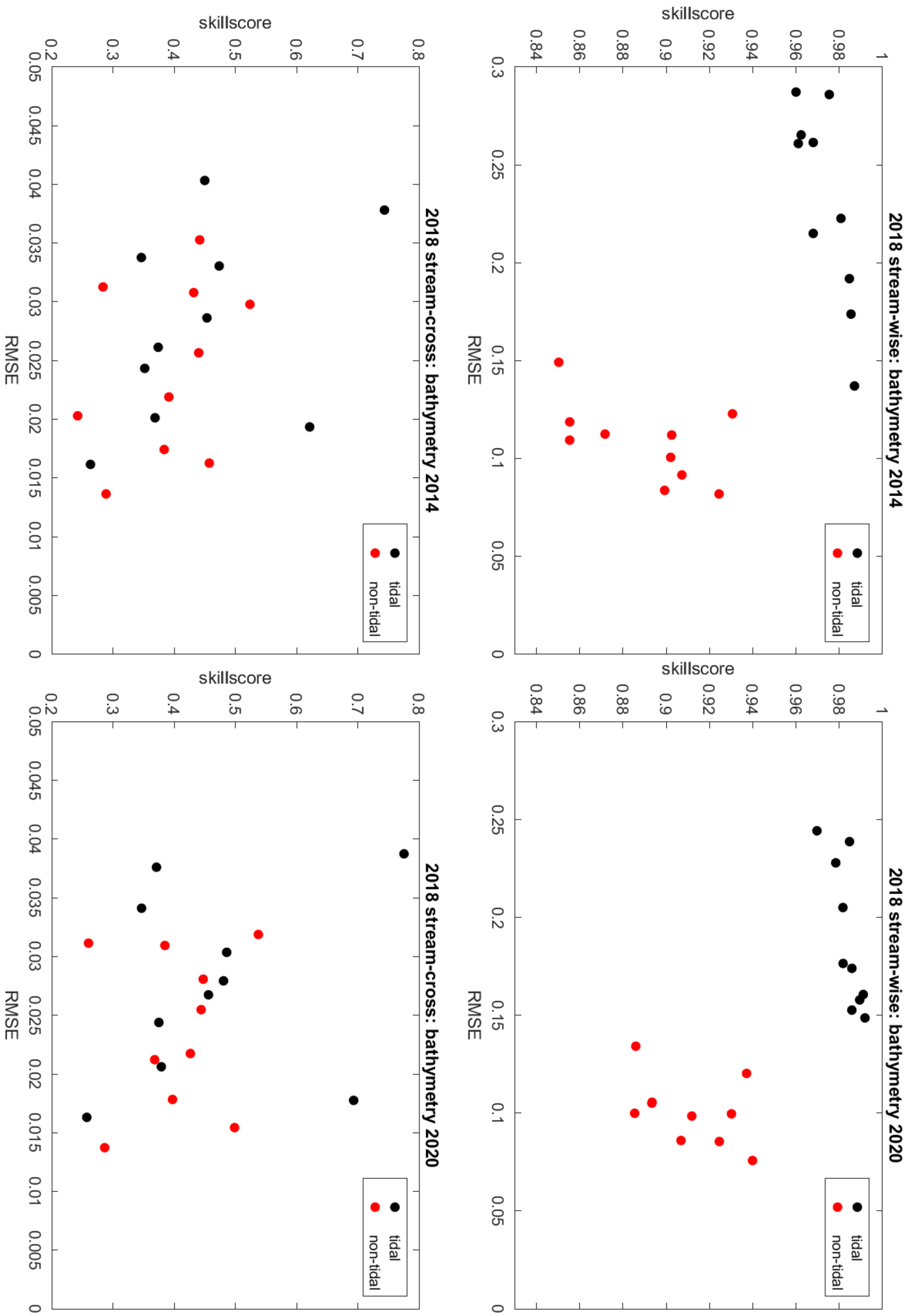
2018 stream-wise: bathymetry 2014
2018 stream-wise: bathymetry 2020
2018 stream-cross: bathymetry 2014
2018 stream-cross: bathymetry 2020
skillscore
RMSE
tidal
non-tidal

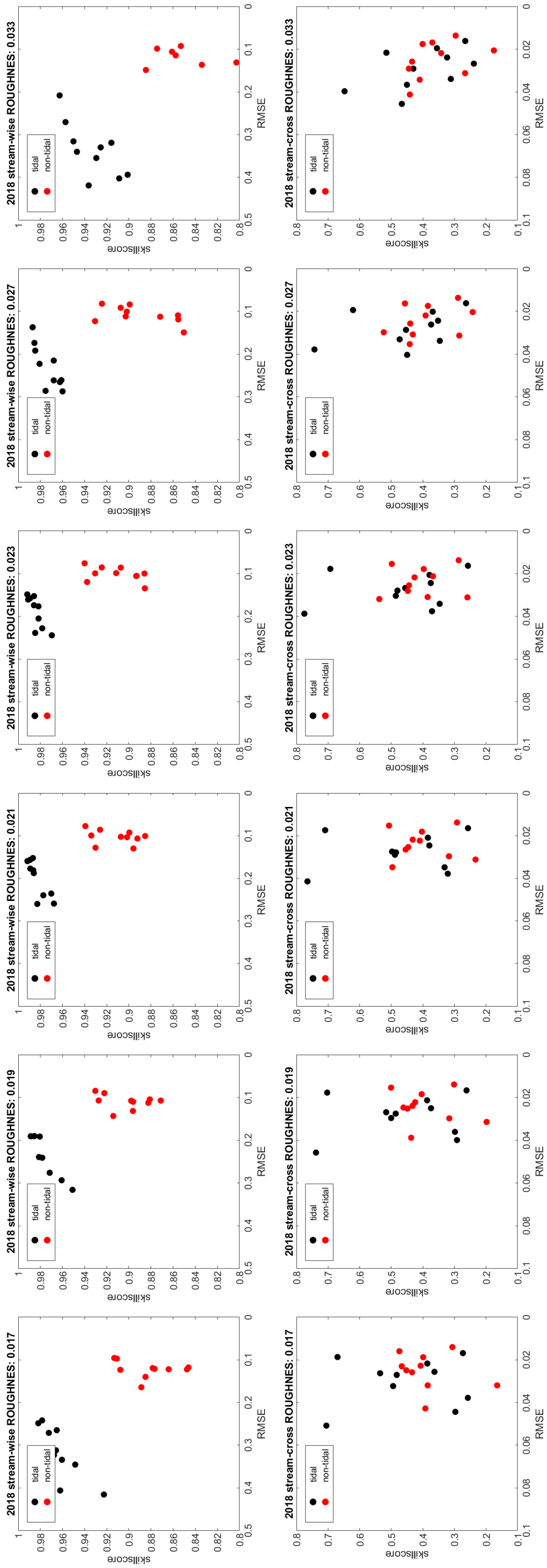
2018 stream-wise ROUGHNES: 0.017
2018 stream-wise ROUGHNES: 0.019
2018 stream-wise ROUGHNES: 0.021
2018 stream-wise ROUGHNES: 0.023
2018 stream-wise ROUGHNES: 0.027
2018 stream-wise ROUGHNES: 0.033
2018 stream-cross ROUGHNES: 0.017
2018 stream-cross ROUGHNES: 0.019
2018 stream-cross ROUGHNES: 0.021
2018 stream-cross ROUGHNES: 0.023
2018 stream-cross ROUGHNES: 0.027
2018 stream-cross ROUGHNES: 0.033
tidal
non-tidal
skillscore
RMSE

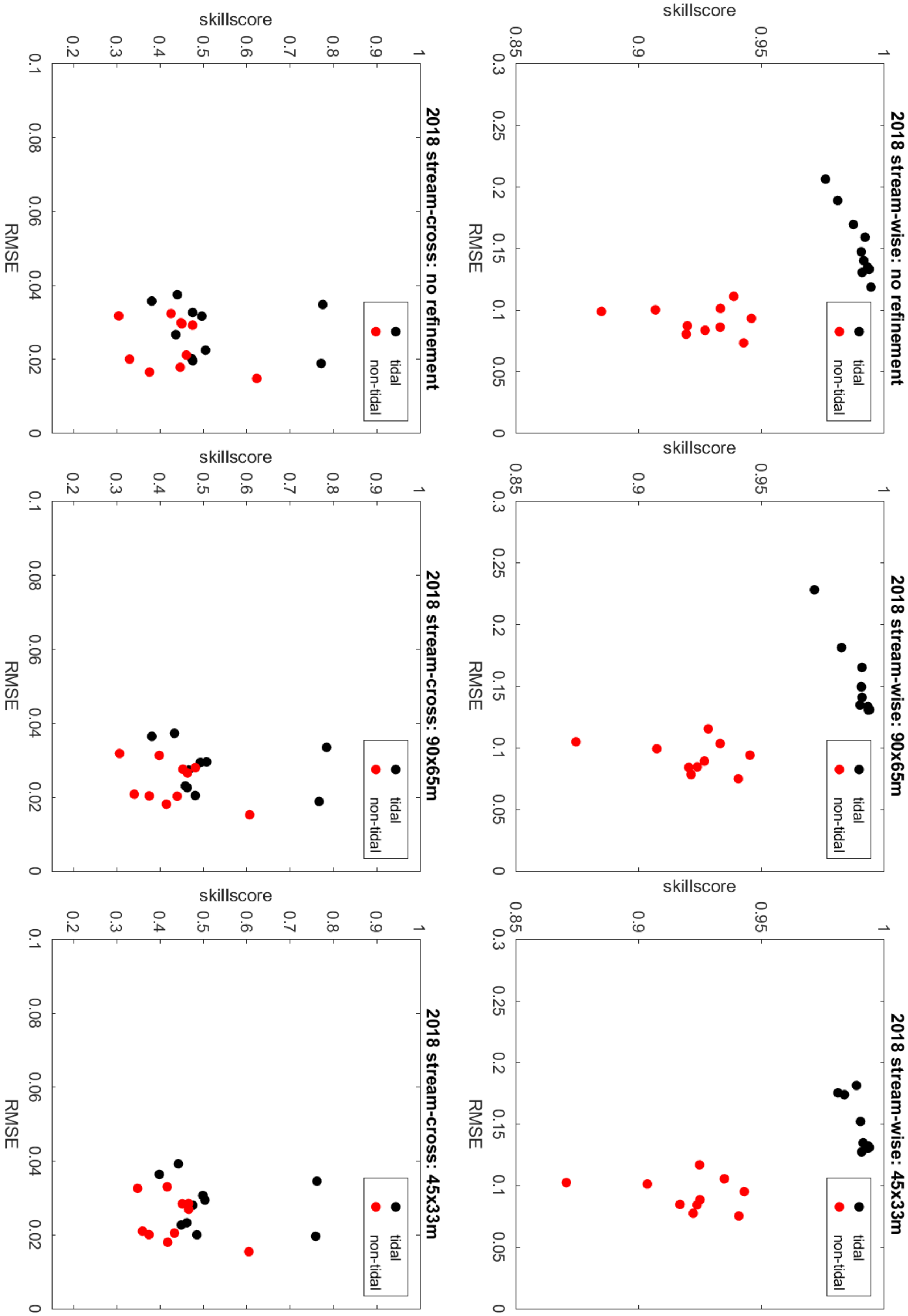
2018 stream-wise: no refinement
2018 stream-wise: 90x65m
2018 stream-wise: 45x33m
2018 stream-cross: no refinement
2018 stream-cross: 90x65m
2018 stream-cross: 45x33m
skillscore
RMSE
tidal
non-tidal

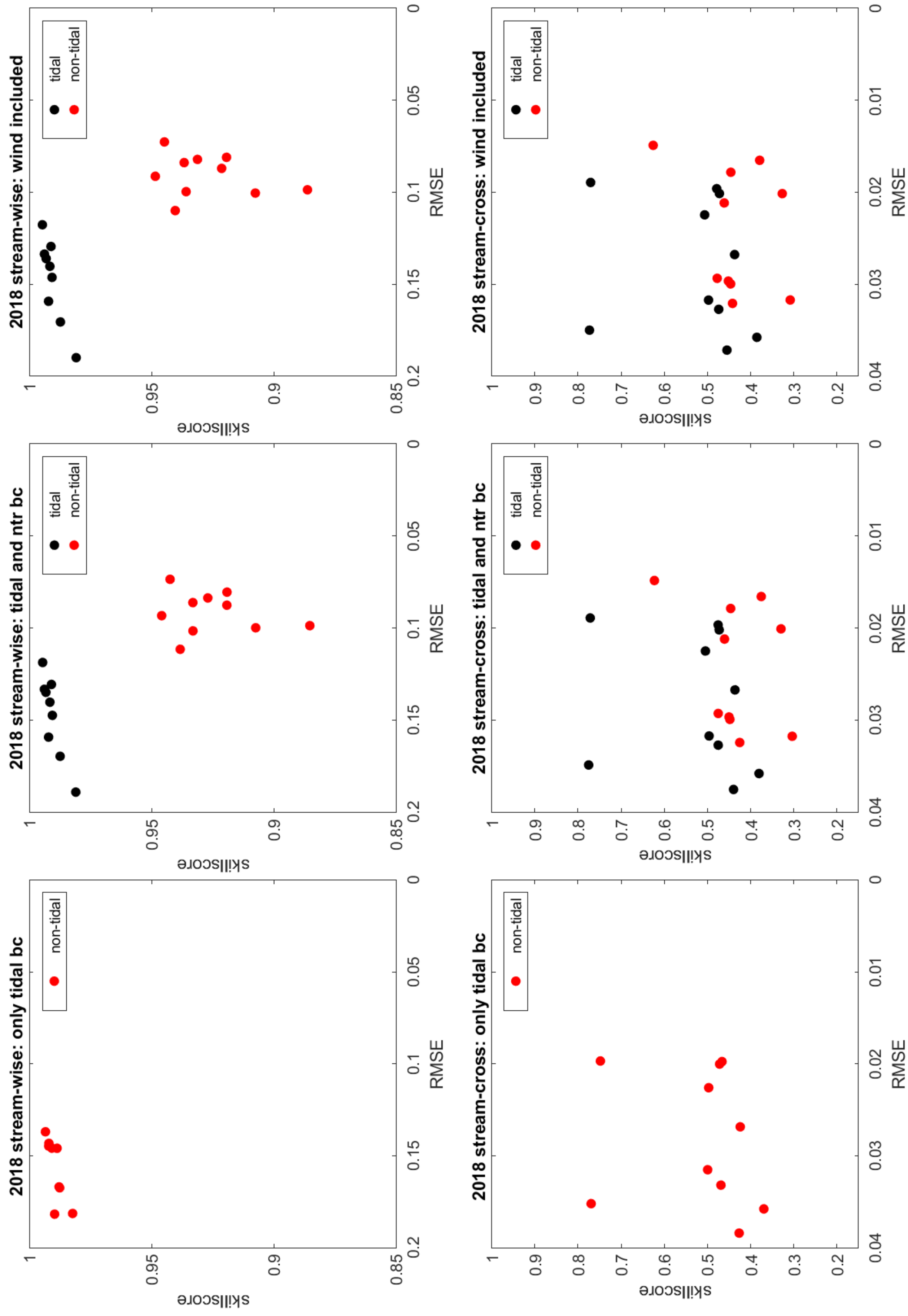
2018 stream-wise: wind included
2018 stream-wise: tidal and ntr bc
2018 stream-wise: only tidal bc
2018 stream-cross: wind included
2018 stream-cross: tidal and ntr bc
2018 stream-cross: only tidal bc
tidal
non-tidal
skillscore
RMSE

Impermeable Dam

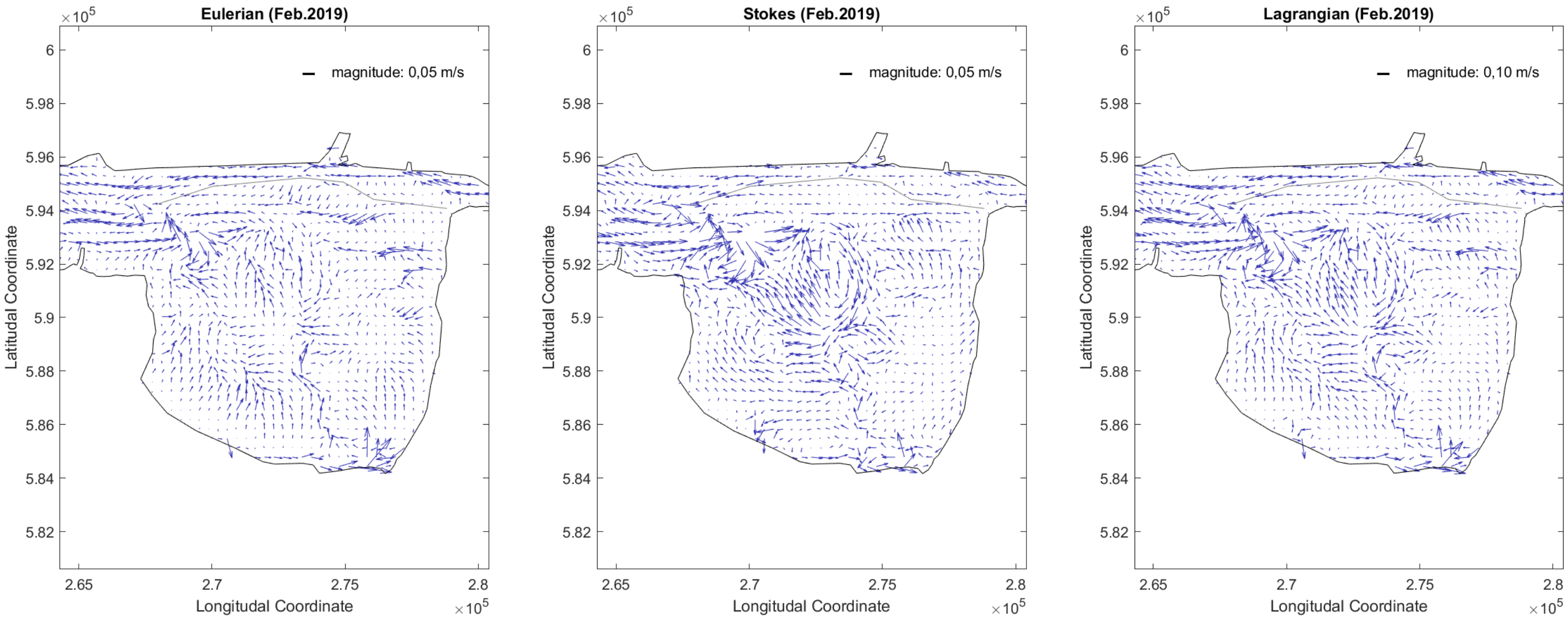

0.0 Meter Dam

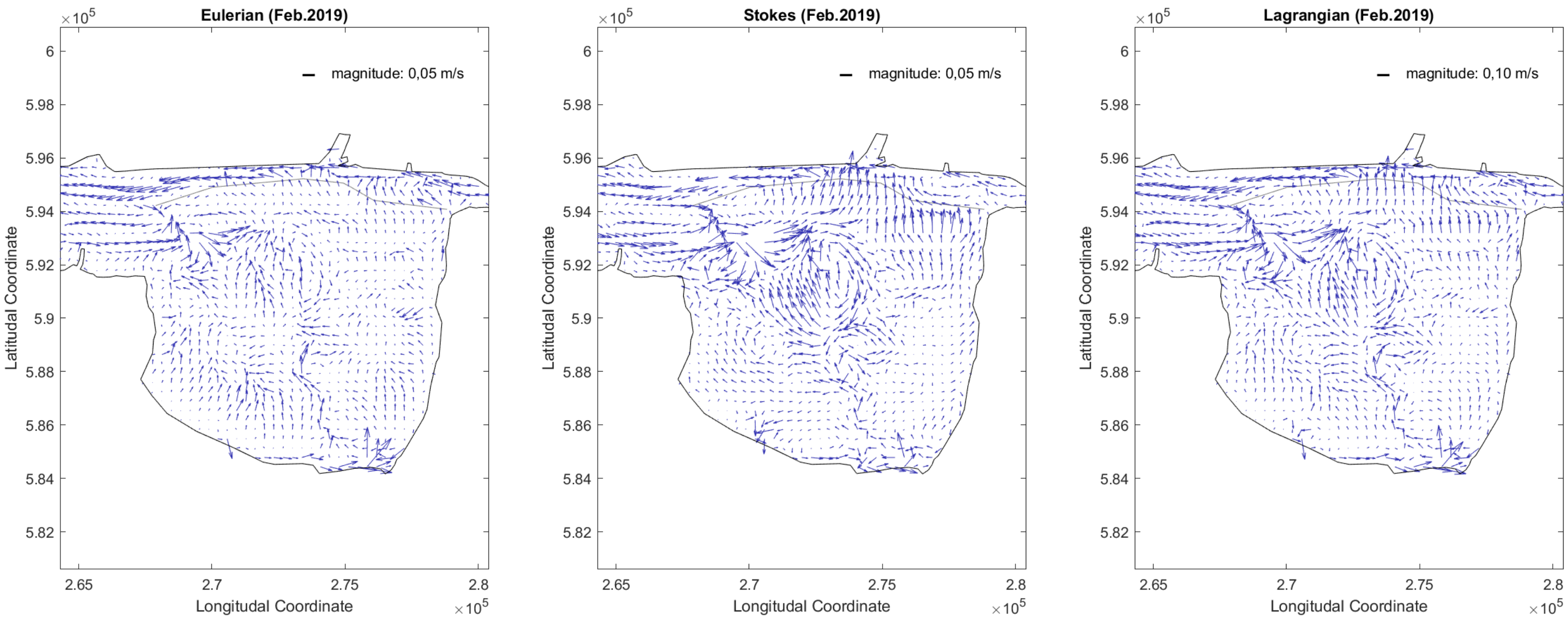

Figure A.5: *The figures above illustrates the influence of Geiseleit Dam on the the Hydrodynamics in terms of the Eulerian, Stokes and Lagrangian flow vecolities. Figure a shows a,b,c respectively show a Eulerian, stokes and Lagrangian velocity vector field.*

0.5 Meter Dam

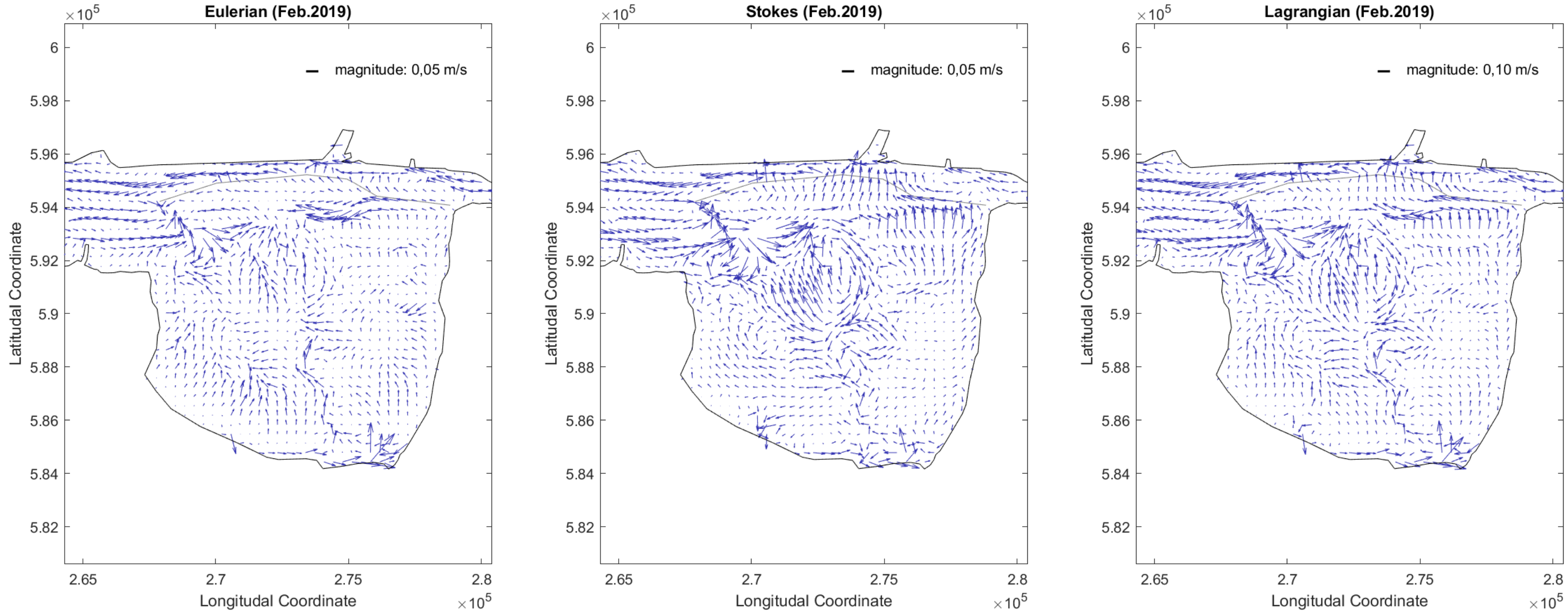

1 Meter Dam

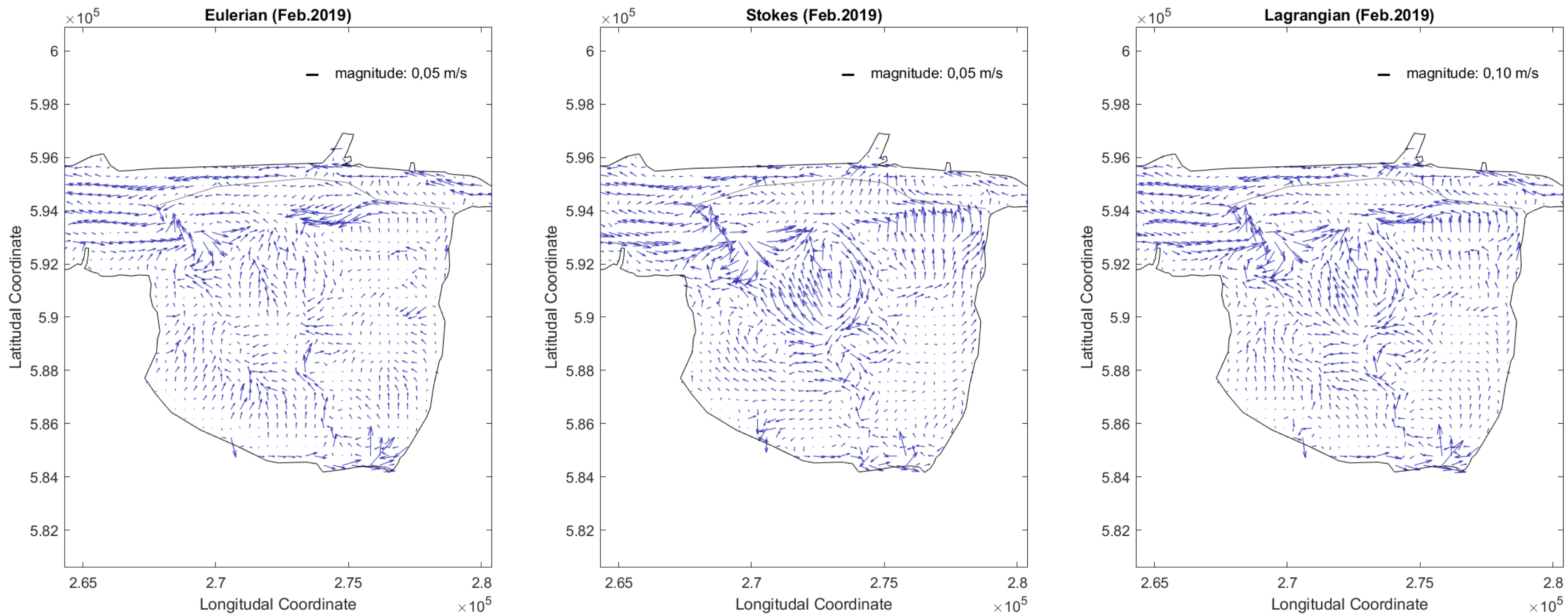

Figure A.6: *The figures above illustrates the influence of Geiseleit Dam on the the Hydrodynamics in terms of the Eulerian, Stokes and Lagrangian flow velocities. Figure a shows a,b,c respectively show a Eulerian, Stokes and Lagrangian velocity vector field.*